1   **Summertime observations of ultrafine particles and cloud**

2   **condensation nuclei from the boundary layer to the free troposphere**

3   **in the Arctic**

4   Julia Burkart[1], Megan D. Willis[1], Heiko Bozem[2], Jennie L. Thomas[3], Kathy Law[3],

5   Peter Hoor[2], Amir A. Aliabadi[4], Franziska Köllner[5], Johannes Schneider[5], Andreas

6   Herber[6], Jonathan P. D. Abbatt[1], W. Richard Leaitch[7]

7   [1]Department of Chemistry, University of Toronto, Toronto, Canada

8   [2]Institute of Atmospheric Physics, Johannes Gutenberg-University, Mainz, Germany

9   [3]LATMOS/IPSL, UPMC Univ. Paris 06 Sorbonne Universités, UVSQ, CNRS, Paris, France

10   [4]Environmental Engineering Program, University of Guelph, Guelph, Canada

11   [5]Particle Chemistry Department, Max Planck Institute for Chemistry, Mainz, Germany

12   [6]Alfred Wegener Institute, Helmholtz Center for Polar and Marine Research, Bremerhaven,
13   Germany

14   [7]Environment and Climate Change Canada, Toronto, Ontario, Canada

15

16   *Correspondence to*: J. Burkart (jburkart@chem.utoronto.ca)

17

18   **Abstract.** The Arctic is extremely sensitive to climate change. Shrinking sea ice extent increases

19   the area covered by open ocean during Arctic summer, which impacts the surface albedo and

20   aerosol and cloud properties among many things. In this context extensive aerosol measurements

21   (aerosol composition, particle number and size, cloud condensation nuclei, and trace gases) were

22   made during 11 flights of the NETCARE July, 2014 airborne campaign conducted from Resolute

23   Bay, Nunavut (74N, 94W). Flights routinely included vertical profiles from about 60 to 3000 m

24   a.g.l. as well as several low-level horizontal transects over open ocean, fast ice, melt ponds, and

25   polynyas.

26   Here we discuss the vertical distribution of ultrafine particles (UFP, particle diameter, dp: 5 – 20

27   nm), size distributions of larger particles (dp: 20 nm to 1 μm), and cloud condensation nuclei

28   (CCN, supersaturation = 0.6%) in relation to meteorological conditions and underlying surfaces.

Atmospheric
Chemistry
and Physics
Discussions

Open Access

EGU

29  UFPs were observed predominantly within the boundary layer, where concentrations were often

30  several hundreds to a few thousand particles per cubic centimeter. Occasionally, particle

31  concentrations below 10 cm$^{-3}$ were found. The highest UFP concentrations were observed above

32  open ocean and at the top of low-level clouds, whereas numbers over ice-covered regions were

33  substantially lower. Overall, UFP formation events were frequent in a clean boundary layer with

34  a low condensation sink. In a few cases this ultrafine mode extended to sizes larger than 40 nm,

35  suggesting that these UFP can grow into a size range where they can impact clouds and therefore

36  climate.

37

38  **1    Introduction**

39  Surface temperatures within the Arctic are rising almost twice as fast as in any other region of the

40  world. As a manifestation of this rapid change the summer sea ice extent has been retreating

41  dramatically over the past decades with the possibility that the Arctic might be ice free by the end

42  of this century (Boé et al., 2009) or even earlier (Wang and Overland, 2012). Increased open ocean

43  is likely to change the properties of both aerosol particles and clouds within the Arctic. Arctic

44  aerosol is well known to show a distinct seasonal variation with maximum mass concentrations

45  and a strong long-range anthropogenic influence in winter and early spring, known as Arctic haze

46  (e.g. Law and Stohl, 2007; Quinn et al., 2007; Shaw, 1995). In contrast, during summer the Arctic

47  is more isolated from remote anthropogenic sources and represents a comparatively pristine

48  environment. The reason is that the Arctic front, which provides a meteorological barrier for lower-

49  level air mass exchange, moves north of many source regions during the summer months.

50  Anthropogenic and biomass burning aerosols are transported to the Arctic during the summer, but

51  at the same time increased aerosol scavenging helps maintain the pristine conditions near the

52  surface  (e.g. Browse et al., 2012; Croft et al., 2015; Garrett et al., 2011).

53  Zhang et al. (2010) discuss the impacts of declining sea ice on the marine planktonic ecosystem,

54  which includes increasing emissions of dimethyl sulfide (DMS) that may contribute to particle

55  formation, such as sulphate particles, in the atmosphere (e.g. Charlson et al., 1987; Pirjola et al.,

56  2000). Enhanced secondary organic aerosol from emissions of biogenic volatile organic

57  compounds is also a possibility (Fu et al., 2009). Primary emissions of aerosol particles from the

Atmospheric
Chemistry
and Physics
Discussions

58    ocean, such as sea salt and marine primary organic aerosol, may also increase (Browse et al., 2014).

59    Open water tends to increase cloudiness, which means that aerosol influences on clouds are likely

60    to be more important. Over the Arctic the effects of aerosols on clouds are especially uncertain.

61    Models have predicted that increasing numbers of particles may lead to overall warming (Garrett,

62    2004) when the atmosphere exists in a particularly low particle number state now referred to being

63    "CCN limited" (Mauritsen et al., 2011), to an overall cooling effect when increasing numbers of

64    particles are added to an atmosphere with more particles already present (Lohmann and Feichter,

65    2005; Twomey, 1974). It is important to characterize particle size distributions in this pristine

66    environment to provide a baseline against which future measurements can be compared in a

67    warming world. Indeed, Carslaw et al. (2013) highlight the need to understand pre-industrial like

68    environments with only natural aerosols in order to reduce the uncertainty in estimations of the

69    anthropogenic aerosol radiative forcing.

70    Primary sources, gas-to-particle formation processes, cloud processing, atmospheric aging, mixing

71    and deposition are all reflected in the size distribution. Therefore, measurements of aerosol size

72    distributions are important for understanding the processes particles undergo in addition to their

73    potential effects on clouds. The presence of ultrafine particles indicates recent production as their

74    lifetime is on the order of hours. We focus this paper on ultrafine particles as these are an indication

75    for in-situ aerosol production processes in the Arctic. We also consider the growth of newly formed

76    particles, as that determines how important they will be for climate.

77    Aerosol size distributions including ultrafine particles ($dp < 20$ nm) have been measured before at

78    different locations throughout the Arctic. Long term studies at ground stations such as Alert

79    (Leaitch et al., 2013), Ny Alesund and Zeppelin (Engvall et al., 2007; Ström et al., 2003, 2009;

80    Tunved et al., 2013), both on Svalbard and very recently in Tiksi, Russia (Asmi et al., 2016) and

81    Station Nord, Greenland (Nguyen et al., 2016) indicate a strong seasonal dependence of the size

82    distribution with the accumulation mode aerosol dominating during the winter months and a shift

83    to smaller particles during the summer months. New particle formation events are frequently

84    observed from June to August.  Ström et al. (2003) show that the size distribution undergoes a

85    rapid change from an accumulation mode dominated distribution (main mode number density:

86    >70nm) during the winter months to an Aitken mode dominated distribution (main mode number

87    density: 30nm) at the beginning of summer. Total number concentrations increase at the beginning

88    of summer and roughly follow the incoming solar radiation on a seasonal scale suggesting that

89    photochemistry is an important factor for new particle formation in the Arctic. At Ny Alesund

90    maximum number concentrations occur in late summer and are explained by the Siberian tundra

91    being a potential source of aerosol precursor gases (Ström et al., 2003). Analysis of air mass

92    patterns for this region show that the shift in the size distributions is also accompanied by a change

93    of source areas, with a dominance of Eurasian source areas in winter and North Atlantic air during

94    summer (Tunved et al., 2013).

95    Ultrafine particle measurements including aerosol size distributions were also conducted from ice

96    breaker cruises such as from the Swedish ice breaker Oden (Bigg and Leck, 2001; Covert et al.,

97    1996; Heintzenberg and Leck, 2012; Leck and Bigg, 2005; Tjernström et al., 2014) and the

98    Canadian Ice breaker Amundsen (e.g. Chang et al., 2011). Chang et al., (2011) use model

99    calculations to show that the appearance of ultrafine particles can be explained by nucleation and

100   growth attributed to the presence of high atmospheric and oceanic DMS concentrations measured

101   at the same time. The Oden expeditions focus on the pack-ice-covered high Arctic, mainly north

102   of 80N and also confirm the frequent presence of an UFP mode (e.g. Covert et al., 1996). The

103   observations from the Oden cruises offer evidence that UFP in the inner Arctic might originate

104   from primary sources (e.g. Heintzenberg et al., 2015; Karl et al., 2013). This is motivated by three

105   main observations. First, a lack of sulfuric acid components in collected 15-50 nm particles (Leck

106   and Bigg, 1999). Second, Leck and Bigg (2010) highlight that nucleation events in the high Arctic

107   do not follow the classical banana shaped growth curve (Kulmala et al., 2001) but enhanced levels

108   of ultrafine particles rather appear simultaneously in distinct size ranges (Karl et al., 2012). Third,

109   the fact that such events cannot be modelled with empirical nucleation mechanisms for the

110   extremely low DMS concentrations in this region (Karl et al., 2013). As a primary source marine

111   microgels are suggested that might become airborne via the evaporation of fog and cloud droplets

112   (Heintzenberg et al., 2006; Karl et al., 2013).

113   So far most studies that include size distribution measurements in the summertime Arctic were

114   conducted from ground stations or ship cruises. To date there are only two studies that asses the

Atmospheric
Chemistry
and Physics
Discussions

115    altitude dependence of the size distribution:, i.e. one in the area of Svalbard (Engvall et al., 2008)

116    and one from the Oden performing vertical profiles with a helicopter (Kupiszewski et al., 2013).

117    In this study we present data from aerosol size distribution measurements taken from an aircraft

118    during a three week period in July 2014 in the high Arctic area of Resolute Bay, Nunavut, Canada.

119    The flights focused on vertical profiles from as low as 60 m above the ground up to 3km, as well

120    as on low-level flights above different terrain such as fast ice, open ocean, polynyas and clouds.

121    We focus especially on UFP (5-20 nm) and address the following questions: What are the

122    concentrations of UFPs in the Arctic summertime, and what is their vertical distribution? What

123    are the environmental conditions that favour occurrence of UFPs? And, is there evidence for

124    growth of UFP to CCN sizes? Aside from the studies conducted near Svalbard, we believe this is

125    the first aircraft study in the high Arctic to systematically address these specific questions. This

126    work provides a comprehensive picture of UFPs observed during the campaign whereas a prior

127    publication from Willis et al., (2016) detailed one UFP formation and growth event observed over

128    Lancaster Sound.

129

## 130    2   Experimental

### 131    2.1   Sampling Platform Polar 6

132    The research aircraft Polar 6 owned by the Alfred Wegener Institute, Helmholtz Center for Polar

133    and Marine Research, Bremerhaven, Germany served as the sampling platform. The Polar 6 is a

134    converted DC-3 airplane (Basler BT-67) modified to work under extreme cold weather conditions.

135    An advantage of the plane is that flights at very relatively low speeds and altitudes (< 60 m a.g.l.)

136    are possible. The cabin of the aircraft is non-pressurized. We maintained a constant survey speed

137    of approximately 120 knots (222 km h$^{-1}$) for measurement flights at constant altitude, and ascent

138    and descent rates of 150 m min$^{-1}$ for vertical profiles. Instruments and measurements specific to

139    this paper are described below.

Atmospheric
Chemistry
and Physics
Discussions

### 2.1.1  Inlets

140

141    Aerosol was sampled through a stainless steel inlet mounted to the top of the plane and ahead of

142    the engines to exclude contamination. The tip of the inlet consisted of a shrouded diffuser that

143    provided nearly isokinetic flow. Inside the cabin the intake tubing was connected to a stainless

144    steel tube (outer diameter of 2.5 cm, inner diameter of 2.3 cm) that carried the aerosol to the back

145    of the aircraft where it was allowed to freely exhaust into the cabin so that the system was not

146    over-pressured. The stainless steel tube functioned as a manifold, off which angled inserts were

147    used to connect sample lines to the various instruments described below. In-flight air was pushed

148    through the line with a flow rate of approximately 55 L min$^{-1}$ determined by the sum of the flows

149    drawn by the instruments (35 L min$^{-1}$), plus the flow measured at the exhaust of the sampling

150    manifold (20 L min$^{-1}$).  A flow of 55 L min$^{-1}$ was estimated to meet nearly isokinetic sampling

151    criteria at survey speed and the transmission of particles through the main inlet was approximately

152    unity for diameters between 20 nm to 1 µm.

153    Trace gases (CO and H$_2$O) were sampled through a separate inlet made of a 0.4 cm (outer diameter)

154    Teflon tube entering the aircraft at the main inlet and exiting through a rear-facing 0.95 cm exhaust

155    line that provided a lower line pressure. The sample flow of approximately 12 L min$^{-1}$ was

156    continuously monitored.

### **2.2   Instrumentation**

157

### 2.2.1  Meteorological parameters and state parameters

158

159    Aircraft state parameters and meteorological measurements were performed with an AIMMS-20

160    manufactured by Aventech Research Inc. at a very high sampling frequency (>40Hz). The

161    AIMMS-20 consists of three modules: (1) The Air Data Probe that measures the three-dimensional

162    aircraft-relative flow vector (true air speed, angle-of-attack, and sideslip), and turbulence with a

163    three-dimensional accelerometer. As well, temperature and humidity sensors are contained within

164    this unit and provide an accuracy and resolution of 0.30 and 0.01 C for temperature and 2.0 and

165    0.1% for relative humidity measurements. (2) An Inertial Measurement Unit that consists of three

166    gyros and three accelerometers providing the aircraft angular rate and acceleration; (4) A Global

167    Positioning System for aircraft 3D position and inertial velocity. Horizontal and vertical wind

168    speeds were measured with accuracies of 0.50 and 0.75 m s$^{-1}$, respectively. The high frequency

169    raw data were processed to 1Hz resolution. Further details of the AIMMS including data

170    processing can be found in (Aliabadi et al., 2016a).

### 2.2.2  Aerosol physical and chemical properties

172    Particle number concentrations and particle size distributions were measured with a TSI 3787

173    water-based ultrafine Condensation Particle Counter (UCPC), a Droplet Measurement Technology

174    (DMT) Ultra High Sensitivity Aerosol Spectrometer (UHSAS) and a Brechtel Manufacturing

175    Incorporated (BMI) Scanning Mobility System (SMS) coupled with a TSI 3010 Condensation

176    Particle Counter (CPC). The UCPC detected particle concentrations of particles larger than 5nm

177    in diameter with a time resolution of 1 Hz. The flow rate was set to 0.6 L min$^{-1}$. The particle

178    concentrations measured by the UCPC are referred to as $N_{tot}$ hereafter.

179    The BMI SMS was set to measure particle size distributions from 20nm to 100nm with a sample

180    flow of 1 L min$^{-1}$ and a sheath flow of 6 L min$^{-1}$. The duration of one scan was 40 s with a 20 s

181    delay time before each scan resulting in a time resolution of 1min.  The UHSAS performed size

182    distribution measurements from 70 nm – 1 µm at a time resolution of 1 Hz with a sample floe rate

183    of 55 cm$^3$ min$^{-1}$. Details of the calibrations and instrument inter-comparisons performed prior and

184    during the campaign are described in detail in Leaitch et al. (2016).

185    Cloud condensation nuclei (CCN) were measured with a DMT CCN Counter (CCNC). The CCNC

186    was operated behind a constant pressure inlet that was set to 650 hPa. The nominal supersaturation

187    was held constant at 1%. Calibrations prior and during the campaign (for details see Leaitch et al.

188    2016) showed that a nominal supersaturation of 1% at the reduced pressure translated into 0.6%

189    effective supersaturation.

190    Cloud droplet sizes from 2-45 µm were measured using a wing mounted Particle Measuring

191    System (PMS) FSSP 100. In this study these data are only used to identify periods when the aircraft

192    was flying in cloud. To avoid possible artefacts produced from shattering of cloud droplets at the

193    aerosol inlet, data from in-cloud times are discarded for the purposes of this study.

194    A DMT Single Particle Soot Photometer (SP2) was deployed to measure refractory black carbon

195    (rBC) number and mass concentrations. We refer to rBC mass concentrations as an indication of

Atmospheric
Chemistry
and Physics
Discussions

196  pollution influence. Calibrations with Aquadag soot were performed prior to and during the

197  campaign. The lower size limit of detection of rBC particles by the SP2 was approximately 80nm.

198  Sub-micron aerosol composition was measured with an Aerodyne high-resolution time-of-flight

199  aerosol mass spectrometer (HR-ToF-AMS; e.g. DeCarlo et al., 2006). A detailed description of

200  the instrument is found in Willis et al. 2016. The main purpose of the instrument was to measure

201  non-refractory particulate matter such as sulphate, nitrate, ammonium, methane sulfonic acid

202  (MSA) and the sum of organics. Lower detection limits were 0.009, 0.008, 0.004, 0.005 and 0.08

203  $\mu g\ m^{-3}$, respectively, and ~70 nm with respect to size in case of ammonium nitrate particles.

204

205  ### 2.2.3  Trace gases

206  Carbon monoxide (CO) was measured with an Aerolaser ultra-fast carbon monoxide monitor

207  model AL 5002 based on VUV fluorimetry, employing the excitation of CO at 150 nm. In-situ

208  calibrations were performed during flight at regular intervals (15 – 30 min) using a NIST traceable

209  CO standard with zero water vapor concentration. CO mixing ratios were used as a relative

210  indicator of aerosol influenced by pollution sources.

211  Water vapour ($H_2O$) measurements were based on infrared absorption using a LI-7200 enclosed

212  $CO_2/H_2O$ Analyzer from LI-COR Biosciences GmbH. The measurement uncertainty is $\pm$ 15 ppm$_v$.

213  $H_2O$ mixing ratios were used to calculate relative humidity with pressure and temperature

214  measured by the AIMMS-20.

215  ## 2.3  Data analysis and nomenclature of particle size data

216  All particle data were averaged to 1 min intervals to match the time resolution of the BMI SMS.

217  Particle concentrations within different size intervals were calculated. The notation $N_{a-b}$ is used;

218  "a" gives the lower limit and "b" the upper limit of the calculated size interval. The BMI SMS was

219  used to determine concentrations of particles from 20-90 nm diameter, and concentrations of

220  particles larger than 90 nm diameter were determined by the UHSAS. If the size interval is

221  expressed as $N_{>a}$ the upper limit is given by the detection limit of the UHSAS (1µm). Additionally,

222  particle concentrations from 5-20 nm (short: $N_{5-20}$) were obtained by subtracting particle

Atmospheric
Chemistry
and Physics
Discussions

223   concentrations measured by the BMI SMS and by the UHSAS from the $N_{tot}$ as determined by the

224   CPC. The $N_{5-20}$ are also referred to as ultrafine particles (UFP) in this study.

225   In order to obtain vertical profiles the data were averaged within altitude intervals. Up to 500 m

226   where 50% of the flight time took place, the averaging interval was 50 m (50-100 m, 100-150 m

227   etc.). Above 500 m, where the data coverage was less, the data were averaged in 100 m altitude

228   bins. The altitude that is reported for a certain interval is given by the average altitude within this

229   intervaland not the middle altitude of the bin interval. Data points in the vertical profiles are

230   therefore not necessarily equidistant but better reflect the actual flying altitude.

231   Average size distributions were obtained by simply averaging each bin for the desired time and

232   altitude range. The size distributions measured by the BMI SMS were used for particle sizes from

233   20-90 nm, and the distributions at larger sizes are taken from the UHSAS. All particle

234   concentrations are expressed for ambient pressure conditions, i.e. they have not been adjusted to

235   standard temperature and pressure conditions. The $N_{5-20}$ referred to as UFP are added to the size

236   distributions as additional bin assuming a bin width of 15 nm (from 5-20 nm) with the mid diameter

237   of 12nm.

238

239   **2.4  FLEXPART-WRF Simulations**

240   We used FLEXPART-WRF (Brioude et al., 2013, website: flexpart.eu/wiki/FpLimitedareaWrf)

241   simulations run backwards in time to analyse the origins of air masses sampled along the flight

242   tracks. FLEXPART-WRF is a Lagrangian particle dispersion model based on FLEXPART (Stohl

243   et al., 2005). Meteorological information is obtained from the Weather Research and Forecasting

244   (WRF) Model (Skamarock et al., 2005). FLEXPART-WRF outputs retroplume information such

245   as the residence time of air (over a unit area) prior to sampling. Residence times were integrated

246   over the entire atmospheric column and 7 days backward in time. FLEXPART-WRF was run in

247   two ways.  First, one FLEXPART-WRF was completed for each flight using particle releases every

248   2 minutes along the flight track (100 m x 100 m x 100 m centered on the aircraft location) to

249   produce potential emissions sensitivities (PES) that represent the average airmass origin for each

250   flight. Second, separate runs were completed for points (every 10 minutes) along the flight track

Atmospheric
Chemistry
and Physics
Discussions

251    (100 m x 100 m x 100 m, 60 second release duration) in order to study different airmasses

252    measured during the same flight. A more detailed description of the model as used for NETCARE

253    2014 is provided by Wentworth et al. (2015).

254

## 2.5   Study area and flight tracks

256    From July 4th to July 21st, 2014 eleven flights were conducted out of Resolute Bay (74.7 N, 95.0

257    W). In Figure 1 a compilation of all flight tracks on a satellite image is shown. The satellite picture

258    was taken on July 4th, 2014 and reflects the situation of the region during period I (July 4 to July

259    12). Resolute Bay proved to be an ideal location for this study as we had access to both open ocean

260    and ice covered regions. Additionally two polynyas were located north of Resolute Bay within the

261    reach of our aircraft. Flights ranged between 4-6 hours. The flights covered two main areas:

262    Lancaster Sound east of Resolute Bay and the area north of Resolute Bay where two polynyas

263    were located. The flights south of Resolute Bay in Lancaster Sound concentrated around the ice

264    edge.

265    The ice/water coverage visible on the satellite picture is representative for the area during the first

266    period. As can be seen, the ice edge was situated about 150 km east of Resolute Bay. It is clearly

267    visible in the satellite image as a sharp line. The transition from a completely ice covered region

268    to open ocean was very abrupt during the first period. Only after a period of bad weather with high

269    winds did the ice edge become less clear, and the region starting about 80 km east of Resolute Bay

270    to about 200 km east was covered by fractured ice.

271    Roughly 50% of the flight time was within the inversion layer, and 50% was in the free troposphere

272    conducting altitude profile flights. A considerable amount of time was spent at 2800 m as this was

273    the preferred altitude when travelling to a certain area. When clouds were present, the aircraft

274    sampled them by slant profiling through the cloud, in the case clouds were above the boundary

275    layer, or, in case clouds were within 200 m of the surface, by descending into the cloud as low as

276    possible. Aerosol observations while inside cloud are excluded from the analysis here due to

277    potential artifacts from droplets shattering on the outside inlet.

278

Atmospheric
Chemistry
and Physics
Discussions

## 3    Meteorological and atmospheric conditions

279

280    Meteorological conditions changed over the course of the campaign. Similar conditions were

281    encountered during the first part of the campaign (July 4th – July 12th, 6 flights), referred to as the

282    "Arctic air mass period" because air masses from within the Arctic dominated and the atmosphere

283    showed structures typical for the Arctic such as a low boundary layer height with thermally stable

284    conditions, indicated by a near surface temperature inversion, and frequent formation of low level

285    clouds. At this time Resolute Bay was under the influence of high pressure systems. Clear sky with

286    few or scattered clouds and low wind speeds dominated. Conditions changed starting from July

287    13th when the region was influenced by troughs of a low pressure system located to the west above

288    Beaufort Sea, which eventually passed through Resolute Bay on July 15th bringing along humidity,

289    precipitation and fog. Intense fog and low visibility impeded flying from July 13th to July 16th. A

290    short good weather window in which the fog dissipated permitted flying again on July 17th

291    (referred to as "transition day"; one flight) just before Resolute Bay came under influence of a

292    pronounced low pressure system located to the south with its center around King William Island

293    (69.0 N, 97.6 W). The last campaign days (referred to as "southern air mass period", three flights)

294    were characterised by the influence of this pronounced low pressure system bringing air masses

295    from the south and providing higher wind speeds, an overcast sky and occasional precipitation.

296    Vertical profiles of median temperature, relative humidity (RH), wind speed, CO and $N_{tot}$ (Figure

297    2) illustrate median atmospheric conditions during the measurement flights. Prominent features

298    representing the trend of each period and reflecting the general meteorological situation will be

299    described here, details discussed in the respective sections. The Arctic air mass period was

300    characterized by frequent thermally stable conditions within the near surface layer , representing

301    typical conditions during the Arctic summertime (Aliabadi et al., 2016a; Tjernström et al.,

302    2012)The median temperature profiles show that on average the boundary layer reached up to

303    ~300 m with a temperature increase of about 5 C. In this paper we will refer to this part of the

304    atmosphere as the boundary layer (BL) and to the air masses above as the free troposphere (FT).

305    A BL height of 300m corresponds well to the boundary layer height of 275 +/- 164 m estimated

306    by (Aliabadi et al., 2016a) using the method of bulk Richardson number (Aliabadi et al., 2016b)

307    and a critical bulk Richardson number of 0.5, using data from radiosondes launched at Resolute

308   Bay and the Amundsen icebreaker, which also performed research operations in Lancaster sound

309   during the campaign period.

310   Within the BL particle concentrations spanned over a wide range of concentrations (max $N_{tot}$:

311   ~10000; median values: ~150 to ~1700 cm$^{-3}$). Highest $N_{tot}$ occurred during the Arctic air mass

312   period, while $N_{tot}$ was constantly low within the lower atmosphere on the transition day. Median

313   temperatures near the surface ranged from -1-5 C during the Arctic air mass period, largely

314   depending on the terrain below (e.g. ice or open water) and were clearly higher when the southern

315   air masses arrived (e.g. at the "surface": 4 C and 7 C, respectively). The higher temperatures

316   coincide with the influence of low pressure systems bringing warmer air masses from the west and

317   south and additional higher wind speeds providing a better mixing of the atmospheric layers (5.6

318   ms$^{-1}$ vs 12m$^{-1}$ near the surface). CO mixing ratios were extremely low during the Arctic air mass

319   period (median: 78.3 ppb$_v$) and on the transition day (median: 83.4 ppb$_v$) indicating pristine air

320   masses that had not recently been affected by pollution or biomass burning sources. The low CO

321   values are representative of background summer conditions (Law et al., 2014). During the southern

322   air mass influence CO mixing ratios clearly increased (median: 95.0 ppb$_v$) confirming a change in

323   air mass and suggesting possible influences by pollution sources and wild fires in the North West

324   Territories (Supplementary Figure 2). Relative humidity profiles show that the near surface layer

325   of the atmosphere was very moist with RH > 80 % during all periods.

326

327   **4   Results and Discussion**

328   **4.1   Ultrafine particle events**

329   4.1.1   Frequency of ultrafine particle events

330   Throughout the campaign we observed large variability in particle concentrations (Figure 3). We

331   observed not only very clean air masses with $N_{tot}$ of a few tens cm$^{-3}$ (with the lowest 1-second

332   value of 1 cm$^{-3}$), but also concentrations as high as a few thousands per cm$^{-3}$ (with the highest

333   value of 10 000 cm$^{-3}$). The highest and lowest concentrations were measured within the BL (Figure

334   3b). Above the BL (Figure 3b) particle concentrations were relatively constant where 60 % of the

Atmospheric
Chemistry
and Physics
Discussions

335    time concentrations were between 200-300 cm$^{-3}$ (for a discussion of the average size distribution

336    see sections 4.1.2 - 4.1.4). Especially during the Arctic air mass period (Figure 2) the atmosphere

337    was characterized by a strong contrast between the BL and the FT.

338    UFP were very frequently present within the BL in high concentrations (Figure 3c). Bursts of $N_{5-20} > 2000/cm^3$

339    were observed over polynas, in Lancaster Sound and south of Resolute Bay. The $N_{5-20}$

340    was higher than 200 cm$^{-3}$ during 65 % of the time. Indeed, high $N_{tot}$ was mainly driven by UFP

341    (as can be seen by comparison of black dots indicating high $N_{tot}$ in Figure 3c and high UFP in

342    Figure 3d). Whenever $N_{tot}$ is greater than 2000 cm$^{-3}$, UFP was at least larger than 1000 cm$^{-3}$. This

343    is also illustrated by the ratio of UFP/$N_{tot}$ (Figure 3e). A ratio of 0 means that no UFP were present,

344    while a ratio of 1 means that only UFP were present. Within the boundary layer 32 % of the time

345    the size distribution was dominated by UFP (ratio > 0.5).

346    The frequent presence of UFP agrees well with other studies made during the Arctic summertime

347    at several locations, such as at the ground stations in Ny Alesund and Zeppelin (Ström et al., 2009;

348    Tunved et al., 2013), at Alert (Leaitch et al., 2013), also from ship-based observations (Chang et

349    al., 2011; Covert et al., 1996; Heintzenberg et al., 2006). However, such a frequent presence of an

350    UFP mode (65 % of the time > 200 cm$^{-3}$) in the BL is unique to this study. Possible reasons for the

351    higher occurrence of UFP might be the combination of the proximity of open ocean (providing a

352    source of UFP or precursor gases), favourable meteorological conditions (sunny weather, inversion

353    layer with cloud formation) and very clean air masses with low condensation sinks. Calm weather

354    conditions may have been another factor. The highest concentrations of UFP were measured at

355    lower wind speeds (< 5 m s$^{-1}$; Supplementary Figure 1), while lower UFP concentrations (1000

356    cm$^{-3}$) were found at high wind speeds (>12 ms$^{-1}$) suggesting a dilution effect of the wind.

357    In the following sections, the vertical distribution of UFP and the size distributions are discussed

358    in relation to meteorological conditions during the three distinct periods that characterized this

359    campaign.

360

Atmospheric
Chemistry
and Physics
Discussions

### 4.1.2 Arctic air mass period: July 4th to July 12th

During this first period the study area was under the influence of a high pressure system. As illustrated by FLEXPART-WRF results (Figure 4a and 4b), air masses were either coming from the North extending to the East in the Arctic Ocean or from the East passing over the open ocean in Lancaster Sound and Baffin Bay. Both examples indicate that air masses resided within the Arctic region at least 5 days prior to sampling. This is true for all flights during this period. The very low CO mixing ratios (78 ppb$_v$, see Figure 2) and average BC mass concentrations of 3 ng m$^{-3}$ (not shown) confirm that air masses were very clean and without recent influence from pollution sources. As discussed in section 3, temperature profiles indicate thermally stable conditions in the lowest layers with near-surface temperature inversions. During almost all vertical profiles we observed temperature inversions of about 4-6 C near the surface. Such an atmospheric structure i.e. a shallow boundary layer is typical for the Arctic summertime (e.g. Aliabadi et al., 2016a; Tjernström et al., 2012).

The Arctic air mass period was characterized by a very sharp contrast between the BL and the FT in terms of particle number concentrations and sizes (Figure 5). The BL was characterized by a prominent layer of UFP from the surface to 300 m (Figure 5a). The height of the UFP layer coincides with the average height of the temperature inversion for this period (see temperature profile Figure 2) and indicates that air masses were stably layered enabling only little exchange with the FT. This is supported by the observed lower turbulent mixing (i.e. turbulent kinetic energy) from boundary layer to the free troposphere during the campaign (Aliabadi et al., 2016a).

During this period we measured the highest concentrations of UFPs with the one minute average up to 5300 cm$^{-3}$. On a typical flight several bursts (concentrations suddenly rising from close to zero to several hundreds and thousands cm$^{-3}$) of high UFP concentrations were encountered in the SIL. These "bursts" lasted from a few seconds to several minutes, corresponding to a spatial extent of several hundreds of meters to dozens of kilometers. The large spatial variability is also illustrated by the frequency distribution of UFP in the BL shown in Figure 5c. E.g. 40 % of the time concentrations of UFP were larger than 200 cm$^{-3}$, 11 % of the time larger than 1000 cm$^{-3}$ and 3% of the time even larger than 2000 cm$^{-3}$. Interestingly the highest concentrations are not found right above the surface (i.e. at the lowest flight altitude of around 60 m) but at a higher altitude

390 (140-170 m). In part, that may be due to the fact that very high concentrations of UFP were

391 measured above the top of low-level clouds, to be discussed in Section 4.3. The average $N_{20-40}$

392 follow a similar trend as the UFP and show also an increase in concentrations within the BL. In

393 contrast, concentrations of larger particles ($N_{>40}$, $N_{>80}$, $N_{>150}$) are minimal at the lowest altitude

394 resulting in a very clean BL with low surface areas (~5 $\mu m^2$ $m^{-3}$ and lower). Within the FT particle

395 concentrations were surprisingly uniform and concentrations of UFP were less than 50 $cm^{-3}$ up to

396 1200 m and ~10 $cm^{-3}$ above.

397 In figure 5b the average and median size distribution is shown and illustrates that increases in only

398 UPF above background levels, without larger particles sizes, were very frequent. However, at

399 times high concentrations of particles extended up to about 40nm. This might indicate that at those

400 times particles experienced growth to larger sizes. Such a case will be discussed in Section 4.3.

401 It should also be noted that occasionally a mode of particles larger than 400 nm was present,

402 associated with open water (see Section 4.2) and therefore most likely the product of primary

403 oceanic emissions.

### 404 4.1.3 Transition day on July 17th

405 July 17th marks the transition from a dominance of Arctic air masses to a clear influence from

406 southern air masses. The transition day consist of only one flight in the area of Lancaster Sound,

407 which, however, is especially interesting as we observed a very "clean" air mass (low

408 concentrations of large particles, e.g. $N_{>40}$: 60-100 $cm^{-3}$, see Figure 6), probably as a result of cloud

409 processing and scavenging during the days before that occurred when flying was impossible

410 because of intense fog and cloud formation at Resolute Bay.

411 On this day the low pressure system situated to the west was bringing air masses from the west

412 along the Canadian and Alaskan coastline (Figure 4c). The temperature profile shows an inversion

413 between 650-1000 m possibly indicating a change in air mass. CO mixing ratios (83 $ppb_v$) and BC

414 mass concentrations (3 $ng$ $cm^{-3}$) are still quite low indicating mostly Arctic background conditions.

415 Again we observed a mode of UFP within the near surface layer (Figure 6b) determined by

416 occasional bursts of UFP with concentrations up to 1400-1900 $cm^{-3}$. UFP of 200 $cm^{-3}$ or more

417 were observed about 20% of the time (Figure 6c) with an average concentration of 240 $cm^{-3}$.

Atmospheric
Chemistry
and Physics
Discussions
Open Access
EGU

418    Concentrations of larger particles ($N_{>40}$, $N_{>80}$, $N_{>150}$) increased sharply at about 700 m coinciding

419    with the temperature inversion. The very low concentrations of larger particles ($N_{>40}$: ~70 cm$^{-3}$)

420    below the temperature inversion are very similar to the conditions encountered within the BL

421    during the previous period. Prior to the transition day the air mass below 700 m was likely cleaned

422    by the clouds and fog that had covered the area during the days before the flight. Only a few hours

423    before the start of the flight, the fog had dissipated and also the terminal aerodrome forecast

424    reported a lift of the cloud base from < 100 m to around 450 m. Median and average size

425    distributions indicate a minimum at around 65 nm that might be the result of cloud processing

426    (Hoppel et al., 1994), consistent with the Arctic observations of Heintzenberg et al., (2006).

427    ### 4.1.4  Southern air mass period: July 19th – July 21st

428    During this period the region was under strong influence of a low pressure system centered south

429    of Resolute Bay. FLEXPART-WRF air mass trajectories (Figures 4d and 4e) indicate a prevalence

430    of air masses from the south potentially affected by wild fires (see Supplementary Figure 2). At

431    the beginning of this period on July 19th (Figure 4d), air mass trajectories suggest the strongest

432    influence from the south while towards the end of the period on July 21st (Figure 4e), FLEXPART-

433    WRF indicates that southern air masses mixed with air masses coming off Greenland. Near surface

434    temperatures were higher than during the previous periods (Figure 2) and temperature inversions

435    were less pronounced (2-4 C) and not observed at all locations suggesting a less stable lower

436    atmosphere. On July 19th we encountered the highest wind speeds in the lower atmosphere (16 m

437    s$^{-1}$ within the near surface layer and 20 m s$^{-1}$ slightly above) and also RH was highest (near the

438    surface 91%) and did not drop below 80% throughout the vertical atmosphere. CO mixing ratios

439    were higher than during the prior periods suggesting that the air was at times influenced by

440    pollution or biomass burning.

441    UFP were observed less frequently than during the Arctic air mass period and in lower

442    concentrations (Figure 7). Bursts of UFP above 1000 cm$^{-3}$ occurred only at three locations, all

443    during the flight on July 21st. Average UFP concentrations were only approximately 190 cm$^{-3}$.

444    UFP concentrations of 200 cm$^{-3}$ or higher were detected 31 % of the time below 300m (Figure 7c).

445     The southern air mass period clearly shows different aerosol characteristics within the near surface

446     layer than compared to the Arctic air mass period and the transition day. Average concentrations

447     of particles larger than 40 nm were highest within the boundary layer and decreased with altitude

448     (Figure 7a). This is in sharp contrast to the very clean (with respect to particles larger than 40 nm)

449     boundary layers observed before. Whereas concentrations of particles larger 40nm were around

450     ~100 cm$^{-3}$ and lower during both prior periods, they were as high as 300 cm$^{-3}$ for this period. Even

451     large accumulation mode particles ($N_{>150}$) averaged ~50 cm$^{-3}$ (compared to 10 cm$^{-3}$ for both

452     previous periods). The average size distribution (Figure 7b) illustrates this in detail: both median

453     and average size distributions show a pronounced mode of particles larger than 500 nm within the

454     BL. Primary emissions from the sea spray promoted by the higher surface wind speeds (see Figure

455     2) are likely a factor contributing to the larger particles.

456     During the southern air mass period, three important factors had changed compared to both prior

457     periods. (1) Air mass back trajectories had clearly shifted to the south and potentially transported

458     emissions from wild fires located in the Northwest Territories (Supplementary Figure 2) into the

459     region, which might mix into the boundary layer. (2) The Amundsen ice breaker was present in

460     Lancaster Sound and acted as a local pollution source (Aliabadi et al., 2016c). (3) Wind speeds

461     were higher and the ocean was visibly turbulent with breaking waves that might enhance primary

462     oceanic aerosol emissions. The increased condensation sinks from these potential sources in

463     combination with other factors (e.g. reduced sun light) and relatively low residence times of air

464     masses within the boundary layer (compared to the Arctic air mass period) may explain the

465     relatively low and infrequent concentrations of UFPs.

466     Within the FT the size distributions shows a bimodal character with a minima at around 65 nm,

467     which possibly indicates that the air masses had experienced cloud processing. Hoppel et al.,

468     (1994). This is very likely, given the presence of the low pressure system bringing moist (see RH

469     ~80% in Figure 2) and warmer air masses. Towards smaller particles the size distribution flattens

470     out (median size distribution) with occasional increased concentrations of particles below ~40 nm

471     (average size distribution). This bimodal size distribution is clearly different from the size

472     distribution during the Arctic air mass period when dry air masses from within the Arctic

473     dominated.

## 4.2   UFP occurrence above ice versus water

474   We investigated the potential influence of different terrain on the occurrence of UFP by examining

476   in detail the time periods when we were flying at altitudes at or below 300 m during the Arctic air

477   mass period. We distinguish between three underlying surfaces: ice covered areas (including ice

478   edge and ice covered with melt ponds), open ocean (including polynyas), and low-level clouds

479   (including both cloud above water and cloud above ice). Here we point out that the case "cloud"

480   does not include in-cloud flight times but only flight periods when above cloud top without actually

481   entering the cloud (confirmed by a zero signal in a liquid cloud probe, FSSP100). An altitude of

482   500 m was chosen to include time periods when we were flying above low-level clouds and to

483   capture mostly flights within the boundary layer where a local influence of the terrain below was

484   likely. During the Arctic air mass period the terrain was characterized by a clear separation

485   between ice and open water. East of the ice edge Lancaster Sound was completely ice free, while

486   west of the ice edge the ocean was seamlessly covered by ice (see satellite picture in Figure 1).

487   All profile above different terrain show unique features (Figure 8). Above ice the highest

488   concentrations of UFP (average: 405 cm$^{-3}$) were found nearer the surface (70 m). In the BL over

489   open water as well as just above cloud, the average number concentrations were higher (1025 cm$^{-3}$

490   and 1533 cm$^{-3}$, respectively) and were found at slightly higher altitudes (140 m and 170 m,

491   respectively). The cloud case is particularly interesting as $N_{20-40}$ particles show an increase at the

492   same time as the UFP suggesting that above cloud UFP do not only form but also grow to larger

493   sizes. In the over-ice and over-open water cases the $N_{20-40}$ show a pattern more similar to the larger

494   particles indicating that their appearance is governed by the same processes as the larger ones. For

495   example, the open water case shows an increase for all particle sizes larger than 20 nm right at the

496   surface that might indicate growth of UFP near the surface. In contrast, UFP reach their highest

497   concentration when all other particle sizes reach a minimum. An increased abundance of UFP at

498   lower surface areas supports the hypothesis that UFP form via nucleation of precursor gases.

Atmospheric
Chemistry
and Physics
Discussions

Open Access

EGU

### 4.3 Case study: July 8

499

500 The flight on July 8 provides a case study focussing on UFP above cloud and within the BL during

501 the Arctic air mass period. We consider the altitude dependence of the UFP within the BL in

502 relation to air mass history and the possible connection with cloud.

503 On this flight we first flew out into Lancaster Sound west of Resolute Bay, turned around and

504 descended into the BL above ice. Here, we focus on the time period from 15:50 UTC (descent into

505 the BL) to 17:20 UTC where we travelled from west to east and remained within the BL but stayed

506 out of cloud ( Figure 9; see also Supplementary Figure 2 for the flight track shown on a satellite

507 image). The later part of the flight focused on in-situ cloud properties and is discussed elsewhere

508 (Leaitch et al., 2016). The weather was sunny with low level clouds starting around 150 km over

509 ice and west of the ice edge in Lancaster Sound. The clouds had formed over the water and were

510 blown over the ice where they partly dissipated (Leaitch et al., 2016). In the entire area the

511 atmosphere was characterized by a surface temperature inversion extending vertically up to about

512 300 m with ~1 C near the surface and ~5 C at 300 m and was accompanied by decreasing relative

513 humidity (Figure 9f). Local low-level winds were dominantly coming from the south to east sector

514 (Figure 9g) and wind speeds were below 5 ms$^{-1}$.

515 UFP were present throughout the BL with the highest concentrations at the lower altitudes and

516 decreasing concentrations towards the top of the BL (Figure 9b). In contrast, larger particles (e.g.

517 $N_{>40}$) exhibit the opposite pattern, with lower concentrations at lower altitudes and higher

518 concentrations at higher altitudes. Six locations from west to east (points A-F in Figure 9a) are

519 used to illustrate the changing aerosol characteristics. Location A is situated well above the BL

520 and at this point no UFP were present (detailed size distributions are shown in Supplementary

521 Figure 4). At location B, the point at which we first entered the BL, an UFP mode (~370 cm$^{-3}$) was

522 present at 60m, while UFP concentrations were lower at slightly higher altitudes (~80 cm$^{-3}$ at 230

523 m) such as location C. At the lower altitudes the UFP mode gradually increased as we approached

524 the ice edge. The most striking observation is the steep increase in particle concentrations at about

525 60 km west of the ice edge (location D) at altitudes of 100-150 m. UFP increased to above 4000

526 cm$^{-3}$ at 150 m. At the same time $N_{20-40}$ concentrations showed a similar increase which was not the

527 case before. At this point we were just above the thickened cloud layer. Notably, increased UFP

528  concentrations were limited to the vicinity of cloud top and decreased rapidly with increasing

529  altitude. Further east (after 1700 UTC, point F) we were restricted to above cloud top and close to

530  the top of the SIL and no peaks of aerosol concentrations were observed with the exception of just

531  before the ice edge (location E).

532  In order to interpret these observations, air mass histories at these locations were investigated with

533  FLEXPART-WRF (Figure 10) and indicate the following:

534  (1) To the west of Resolute Bay (point B) Lancaster Sound air masses had been mixed with air

535  masses from the North. This is also confirmed by the local wind directions indicating winds

536  coming from the Northwest sector (Figure 10a), and it is consistent with the associated change in

537  cloud. (2) Towards the top of the BL air masses had descended only very recently ($< 3$ h) into the

538  SIL from above the BL (Figure 10c point C and point F). (3) In contrast, deeper within the BL

539  such as at point ii and at point iv air masses had descended into the BL earlier (~20 h) before

540  arriving at the point of observation. In the case of point D, where we observed the largest mode of

541  UFP extending above 40nm, air masses had been travelling from the east exclusively over the open

542  waters in Lancaster Sound during the last day before arriving at the point of observation (Figure

543  10b, point D).

544  Aerosol composition shows a clear difference between the aerosol in the FT and the BL. The

545  aerosol sulphate rapidly decreases as we enter the BL around 16:00, while aerosol organic loadings

546  show an initial relative increase followed by an absolute increase towards the east (Figure 9c).

547  Within the BL aerosol organics and sulphate mass loadings show a pattern similar to $N_{>40}$ and

548  $N_{>80}$. Both decrease each time we descended deeper into the BL. However, at the same time the

549  organics-to-sulphate ratio indicates that the relative contribution of organics to aerosol mass

550  increases at lower altitudes and especially above cloud (Figure 9e). Well within the inversion layer

551  and in the vicinity of cloud top the aerosol was dominated by organics. At the same time also ratio

552  of MSA to sulphate was higher (Figure 9e), suggesting a marine biogenic influence of the aerosol

553  sulphur. The marine biogenic influence at the lower altitudes agrees well with the FLEXPART-

554  WRF simulations showing that air masses at this altitude had spent almost an entire day exposed

555  to the open waters in Lancaster Sound. For a more detailed discussion of organic aerosol and

556  growth see (Willis et al., 2016) and references therein.

557 Consistent with the higher organic content measured with the AMS, the single particle aerosol

558 mass spectrometer ALABAMA (Brands et al., 2011; Willis et al., 2016) detected a higher fraction

559 of trimethylamine (TMA)-containing particles for particles larger than 150 nm in diameter.

560 Gaseous TMA emissions from marine biogenic origin (Ge et al., 2011; Gibb et al., 1999) may have

561 additionally favored the subsequent growth of the freshly nucleated particles by condensation.

562 Another possibility may be uptake of TMA in the cloud phase (Rehbein et al., 2011) if the particles

563 have grown to sufficiently large sizes to be activated as CCN. Interestingly, compared to other

564 days these TMA-containing particles are smaller and to a lesser degree internally mixed with

565 potassium and levoglucosan which supports the hypothesis of ultrafine particles originating from

566 nucleation in a biogenic marine environment and subsequent growth. A detailed discussion of

567 TMA-containing particles observed during this campaign will be presented in (Köllner et al., 2016

568 in prep).

569 To explain these observations, we hypothesize that the smaller particle mode is formed by

570 nucleation and growth occurring within the BL and especially in cloud vicinity. UFP

571 concentrations near cloud top have been reported before (e.g. Garrett et al., 2002; Hegg et al.,

572 1990) and it is suggested that nucleation in near cloud regions is favoured by the low surface areas

573 in cloud scavenged air masses, moist air and a high actinic flux. Indeed, in cloud vicinity where

574 we observed an increase of UFP extending up to almost 50nm the conditions for nucleation and

575 growth are ideal: we speculate that the availability of precursor gases is provided by the long

576 residence time (~20h) of the air masses over open water. The very high organic loadings and MSA

577 to sulphate ratio likely indicate that the formation of these particles is driven by organic precursors.

578 Precursor gases such as DMS and volatile organic compounds (VOCs) are likely emitted by the

579 open ocean in Lancaster Sound (e.g. Ghahremaninezhad et al., 2016 in prep; Mungall et al., 2016).

580 At first sight the increase of UFP at point E seems to contradict these observations. The event

581 occurs at a point where the aircraft was clearly above cloud and close to the top of the BL, at a

582 location where no increases in UFP were observed before or after. However, at this point we were

583 in vicinity of Prince Leopold Island which is a bird sanctuary and many bird colonies nest at the

584 260m high cliff. FLEXPART-WRF shows that air masses to a large extent were directly coming

585 off the island (Figure 10, point E) suggesting a connection between the appearance of UFP and

Atmospheric
Chemistry
and Physics
Discussions

586    possible emissions from the fauna of the island. The increase of particle phase ammonium, $NH_4$,

587    (Figure 9d) at the same time strongly supports this connection and nucleation of particles from

588    biogenic precursors emitted by bird colonies are documented (Weber et al., 1998; Wentworth et

589    al., 2015, Croft et al. 2016b).

590    Alternatively, it should be considered that evaporating fog and cloud droplets may also act as a

591    primary source of UFP (e.g. Heintzenberg et al., 2006; Karl et al., 2013; Leck and Bigg, 1999).

592    Karl et al., (2013) suggested a combined pathway that involves the emission of UFP by fog and

593    cloud droplets, together with secondary processes enabling growth of these particles. For our

594    observations we have no reason to assume that nucleation does not occur since conditions are ideal

595    but we cannot rule out that nanoparticles are emitted by the possibly evaporating cloud droplets

596    onto which gases then condense.

597    In conclusion the aerosol mass within the near surface layer is dominated by organics relative to

598    sulphate, while at just slightly higher altitude sulphate is clearly increased and increases further

599    above the inversion layer. A high organic content coincides with increases in UFP particles,

600    especially at times when also growth into the size range up to 50nm is indicated. Similarly the

601    MSA-to-sulphate ratio shows a peak at the lowest altitudes with maximum values in the vicinity

602    of clouds that coincide with a long residence time (~20h) of the air masses within the BL and

603    above open water. The data thereby suggest a marine biogenic influence of the aerosol within the

604    lower layers of the atmosphere. We note that similarly high levels of aerosol organics and MSA

605    were observed during the flight on July 12 associated with a NPF event and growth but in cloud-

606    free conditions Willis et al. (2016).

## 4.4 CCN activity

608    CCN concentrations were measured at a supersaturation of 0.6 %. The vertical profiles of CCN

609    concentrations (Figure 11a) show patterns similar to those of larger particles. In the very clean

610    boundary layer of the Arctic air mass period and the transition day CCN concentrations are equally

611    low (~70 $cm^{-3}$ and ~50 $cm^{-3}$, respectively). In contrast, during the southern air mass period average

612    CCN concentrations are amongst the highest observed during this campaign (>300 $cm^{-3}$). Within

613    the free troposphere CCN concentrations are surprisingly constant during the Arctic air mass

Atmospheric
Chemistry
and Physics
Discussions

614    period ($120 \pm 27$ cm$^{-3}$) and more variable on the transition day ($92 \pm 46$ cm$^{-3}$) and the southern air

615    mass period ($103 \pm 67$ cm$^{-3}$). The constant CCN concentrations during the Arctic air mass period

616    correspond to the very uniform atmosphere dominated by aged aerosols we observed during this

617    period and to the more layered atmosphere influenced by southern air masses possibly

618    contaminated by biomass burning plumes during the later period. Correlations with $N_{>80}$ (Figure

619    11b) confirm that larger particles are a good approximation for these CCN concentrations. On

620    average CCN concentrations agree roughly to within $\pm 20$ % of $N_{>80}$ suggesting that a diameter of

621    80 nm is a good approximation for the activation diameter of the aerosol at 0.6 % supersaturation.

622    However, it should be noted that slight differences between the 3 periods are indicated in the

623    correlation curves: during the Arctic air mass period the average activation diameters are smaller

624    than 80 nm, and during the southern air mass period they are larger than 80 nm. Assuming uniform

625    chemical composition throughout the particle size range, an activation diameter of 80 nm at 0.6 %

626    supersaturation indicates an aerosol much less hygroscopic than, for example, ammonium

627    sulphate; pure ammonium sulphate particles would activate at 40 m at 0.6 % supersaturation. For

628    the one specific event during which growth occurred (Willis et al., 2016), it was demonstrated that

629    high CCN concentrations coincide with elevated organic mass loading. The reduced

630    hygroscopicity of organic material (Petters and Kreidenweis, 2007) can explain the larger effective

631    activation diameter.

632

## 633    5   Discussion and Conclusions

634    This study presents airborne observations of ultrafine particles (UFP) during the Arctic

635    summertime. The study of Leaitch et al., (2016) for this same campaign has illustrated the

636    importance of small particles (20 – 100 nm) to cloud formation and thus climate in this region.

637    Eleven flights were conducted in July 2014 in the area of Resolute Bay situated in the middle of

638    the Canadian Archipelago. The location allowed access to open water, ice covered regions and

639    polynyas. Flights focused around the ice edge in Lancaster Sound (7 flights) including the open

640    waters to the east and the ice covered region to the west, and north of Resolute Bay around the

641    polynyas (3 flights). UFP were observed within all regions and above all terrains with the highest

642    concentrations encountered in Lancaster Sound above cloud and open water. UFP observations

Atmospheric
Chemistry
and Physics
Discussions

643     were discussed in relation to different meteorological conditions (Arctic air mass period, transition

644     day, southern air mass period). It is shown that UFP occur most frequently (>65 % of the time)

645     and with the highest concentrations (up to 5300 cm$^{-3}$) during the Arctic air mass period when the

646     air is relatively clean and the  BL thermally stable.

647     The frequent presence of UFP in the BL during the Arctic air mass period over open water and

648     low cloud suggests a surface source for the observed particles, such as the ocean. This is especially

649     true during the Arctic air mass period when the sampling region was experimentally found to be

650     pristine and not influenced by pollution, as confirmed by the FLEXPART-WRF simulations that

651     show air masses had resided within the Arctic region at least 5-7 days prior to sampling. During

652     this time UFP were restricted to the boundary layer and no UFP events were observed aloft, thereby

653     excluding that these UFP might form in the free troposphere and subside into the near surface layer

654     e.g. (Clarke et al., 1998; Quinn and Bates, 2011). At the same time we observed an extremely clean

655     BL (surface area of N$_{>40}$ ~5µm$^2$m$^{-3}$). Low surface areas increase the probability of particle

656     formation via nucleation by reducing the surfaces for precursor gases, such as DMS or VOCs, to

657     condense on. Chlorophyll-a concentrations (Supplementary Figure 5) suggest there was a

658     relatively high level of biological activity of the ocean (such as phytoplankton blooms known to

659     produce DMS) throughout Lancaster Sound, to the east in Baffin Bay and in the open waters of

660     the polynyas during the time period of the study.

661     Measurements of gas phase DMS in Lancaster Sound performed from the Amundsen ice breaker

662     just a few days after the aircraft campaign described in this study show that DMS was ubiquitous

663     in the Lancaster Sound region (Mungall et al., 2016). Mixing ratios ranged from 4-1155 ppt$_v$ with

664     the highest value measured at the east end of Lancaster Sound and a median value of 186 ppt$_v$ (for

665     the entire study time and area including Baffin Bay and Nares Strait). DMS was also measured

666     from the Polar 6 aircraft with an offline technique and also shows a large variability within the BL.

667     Maximum mixing ratios of 110 ppt$_v$ were detected in the surface layer (Ghahremaninezhad et al.,

668     2016 in prep.), again confirming a marine influence in the boundary layer. The measured DMS

669     concentrations are above the nucleation threshold obtained by modelling performed in the study

670     of Chang et al. (2011) who concluded that DMS mixing ratios of ≥ 100 ppt$_v$ are sufficient to

671     account for the formation of hundreds of UFP when background particle concentrations are < 100

Atmospheric
Chemistry
and Physics
Discussions

672    $cm^{-3}$. These conditions agree very well with our observations during Arctic air mass period, when

673    background particle concentrations ($N_{>40}$) within the boundary layer were low.

674    Relating observations of UFP to the surface below (ice, water, low-level cloud) during the Arctic

675    air mass period revealed that the highest UFP concentrations occurred above low-level cloud and

676    open water with averages of 1533 $cm^{-3}$ and 1025 $cm^{-3}$, respectively. Above low-level cloud in

677    addition to UFP also $N_{20-40}$ showed increased concentrations. This simultaneous increase in

678    concentrations suggests that UFP grow into the 40 nm size range.

679    Overall, the summertime Arctic is an active region in terms of new particle formation, occasionally

680    accompanied by growth. The value of the altitude profiles across a wide spatial extent, performed

681    for the first time in this campaign, is that they demonstrate that this activity is largely confined to

682    the boundary layer, and that the dominant source of small particles to the boundary layer does not

683    arise by mixing from aloft but most likely from marine sources. For future studies, the relative

684    impact of such natural sources of UFP needs to be evaluated with respect to potential new sources,

685    such as may arise with increasing shipping.

686

Atmospheric
Chemistry
and Physics
Discussions

Open Access

EGU

Atmospheric
Chemistry
and Physics
Discussions

713    **References**

714    Aliabadi, A. A., Staebler, R. M., Liu, M. and Herber, A.: Characterization and Parametrization of
715    Reynolds Stress and Turbulent Heat Flux in the Stably-Stratified Lower Arctic Troposphere Using
716    Aircraft Measurements, Boundary-Layer Meteorol., doi:10.1007/s10546-016-0164-7, 2016a.

717    Aliabadi, A. A., Staebler, R. M., de Grandpré, J., Zadra, A. and Vaillancourt, P. A.: Comparison
718    of Estimated Atmospheric Boundary Layer Mixing Height in the Arctic and Southern Great Plains
719    under Statically Stable Conditions: Experimental and Numerical Aspects, Atmosphere-Ocean,
720    54(1), 60–74, doi:10.1080/07055900.2015.1119100, 2016b.

721    Aliabadi, A. A., Thomas, J. L., Herber, A., Staebler, R. M., Leaitch, W. R., Law, K. S., Marelle,
722    L., Burkart, J., Willis, M., Abbatt, J. P. D., Bozem, H., Hoor, P., Köllner, F., Schneider, J. and
723    Levasseur, M.: Ship emissions measurement in the Arctic from plume intercepts of the Canadian
724    Coast Guard Amundsen icebreaker from the Polar 6 aircraft platform, Atmos. Chem. Phys., 16,
725    7899–7916, doi:doi:10.5194/acp-16-7899-2016, 2016c.

726    Asmi, E., Kondratyev, V., Brus, D., Laurila, T., Lihavainen, H., Backman, J., Vakkari, V., Aurela,
727    M., Hatakka, J., Viisanen, Y., Uttal, T., Ivakhov, V. and Makshtas, A.: Aerosol size distribution
728    seasonal characteristics measured in Tiksi, Russian Arctic, Atmos. Chem. Phys., 16(3), 1271–
729    1287, doi:10.5194/acp-16-1271-2016, 2016.

730    Bigg, E. K. and Leck, C.: Properties of the aerosol over the central Arctic Ocean, J. Geophys. Res.,
731    106(D23), 32101, doi:10.1029/1999JD901136, 2001.

732    Boé, J., Hall, A. and Qu, X.: September sea-ice cover in the Arctic Ocean projected to vanish by
733    2100, Nat. Geosci., 2(5), 341–343, doi:10.1038/ngeo467, 2009.

734    Brands, M., Kamphus, M., Böttger, T., Schneider, J., Drewnick, F., Roth, a., Curtius, J., Voigt,
735    C., Borbon, a., Beekmann, M., Bourdon, a., Perrin, T. and Borrmann, S.: Characterization of a
736    Newly Developed Aircraft-Based Laser Ablation Aerosol Mass Spectrometer (ALABAMA) and
737    First Field Deployment in Urban Pollution Plumes over Paris During MEGAPOLI 2009, Aerosol
738    Sci. Technol., 45(1), 46–64, doi:10.1080/02786826.2010.517813, 2011.

739    Brioude, J., Arnold, D., Stohl, A., Cassiani, M., Morton, D., Seibert, P., Angevine, W., Evan, S.,
740    Dingwell, A., Fast, J. D., Easter, R. C., Pisso, I., Burkhart, J. and Wotawa, G.: The Lagrangian
741    particle dispersion model FLEXPART-WRF version 3.1, Geosci. Model Dev., 6(6), 1889–1904,
742    doi:10.5194/gmd-6-1889-2013, 2013.

743    Browse, J., Carslaw, K. S., Arnold, S. R., Pringle, K. and Boucher, O.: The scavenging processes
744    controlling the seasonal cycle in Arctic sulphate and black carbon aerosol, Atmos. Chem. Phys.,
745    12(15), 6775–6798, doi:10.5194/acp-12-6775-2012, 2012.

746    Browse, J., Carslaw, K. S., Mann, G. W., Birch, C. E., Arnold, S. R. and Leck, C.: The complex
747    response of Arctic aerosol to sea-ice retreat, Atmos. Chem. Phys., 14(14), 7543–7557,
748    doi:10.5194/acp-14-7543-2014, 2014.

749    Carslaw, K. S., Lee, L. A., Reddington, C. L., Pringle, K. J., Rap, A., Forster, P. M., Mann, G. W.,
750    Spracklen, D. V, Woodhouse, M. T., Regayre, L. A. and Pierce, J. R.: Large contribution of natural
751    aerosols to uncertainty in indirect forcing., Nature, 503(7474), 67–71, doi:10.1038/nature12674,

Atmospheric
Chemistry
and Physics
Discussions

752  2013.

753  Chang, R. Y. W., Sjostedt, S. J., Pierce, J. R., Papakyriakou, T. N., Scarratt, M. G., Michaud, S.,
754  Levasseur, M., Leaitch, W. R. and Abbatt, J. P. D.: Relating atmospheric and oceanic DMS levels
755  to particle nucleation events in the Canadian Arctic, J. Geophys. Res. Atmos., 116(21), 1–10,
756  doi:10.1029/2011JD015926, 2011.

757  Charlson, R. J., Lovelock, J. E., Andreae, M. O. and Warren, S. G.: Oceanic phytoplankton,
758  atmospheric sulphur, cloud albedo and climate, Nature, 326, 655–661, doi:10.1038/326655a0,
759  1987.

760  Clarke, A. D., L, V. J., Eisele, F., Mauldin, R. L., Tanner, D. and M, L.: Particle production in the
761  remote marine atmosphere : Cloud outflow and subsidence during ACE 1, Earth Sci., 103, 1998.

762  Covert, D. S., Wiedensohler, A., Aalto, P., Heintzenberg, J., McMurry, P. H. and Leck, C.: Aerosol
763  number size distributions from 3 to 500 nm diameter in the arctic marine boundary layer during
764  summer and autumn, Tellus, Ser. B Chem. Phys. Meteorol., 48(2), 197–212, 1996.

765  Croft, B., Martin, R. V., Leaitch, W. R., Tunved, P., Breider, T. J., D'Andrea, S. D. and Pierce, J.
766  R.: Processes controlling the seasonal cycle of Arctic aerosol number and size distributions,
767  Atmos. Chem. Phys. Discuss., 15(20), 29079–29124, doi:10.5194/acpd-15-29079-2015, 2015.

768  DeCarlo, P. F., Kimmel, J. R., Trimborn, A., Northway, M. J., Jayne, J. T., Aiken, A. C., Gonin,
769  M., Fuhrer, K., Horvath, T., Docherty, K. S., Worsnop, D. R. and Jimenez, J. L.: Field-deployable,
770  high-resolution, time-of-flight aerosol mass spectrometer., Anal. Chem., 78(24), 8281–9,
771  doi:10.1021/ac061249n, 2006.

772  Engvall,  a.-C., Krejci, R., Ström, J., Treffeisen, R., Scheele, R., Hermansen, O. and Paatero, J.:
773  Changes in aerosol properties during spring-summer period in the Arctic troposphere, Atmos.
774  Chem. Phys. Discuss., 7(1), 1215–1260, doi:10.5194/acpd-7-1215-2007, 2007.

775  Engvall, A.-C., Krecji, R., Sröm, J., Minikin, A., Treffeisen, R., Stohl, A. and Herber, A.: In-situ
776  airborne observations of the microphysical properties of the Arctic tropospheric aerosol during
777  late  spring  and  summer,  Tellus  B,  0(0),  080414161623888–???,  doi:10.1111/j.1600-
778  0889.2008.00348.x, 2008.

779  Fu, P., Kawamura, K., Chen, J. and Barrie, L. A.: Article in the High Arctic Aerosols during Late
780  Winter to Early Summer Sesquiterpene Oxidation Products in the High Arctic Aerosols during
781  Late Winter to Early Summer, , 43(11), 4022–4028, doi:10.1021/es803669a, 2009.

782  Garrett, T. J.: Effects of varying aerosol regimes on low-level Arctic stratus, Geophys. Res. Lett.,
783  31(17), L17105, doi:10.1029/2004GL019928, 2004.

784  Garrett, T. J., Hobbs, P. V and Radke, L. F.: High Aitken Nucleus Concentrations above Cloud
785  Tops  in  the  Arctic,  J.  Atmos.  Sci.,  59(3),  779–783,  doi:10.1175/1520-
786  0469(2001)059<0779:HANCAC>2.0.CO;2, 2002.

787  Garrett, T. J., Brattström, S., Sharma, S., Worthy, D. E. J. and Novelli, P.: The role of scavenging
788  in the seasonal transport of black carbon and sulfate to the Arctic, Geophys. Res. Lett., 38(16), 1–
789  6, doi:10.1029/2011GL048221, 2011.

790  Ge, X., Wexler, A. S. and Clegg, S. L.: Atmospheric amines - Part I. A review, Atmos. Environ.,

791    45(3), 524–546, doi:10.1016/j.atmosenv.2010.10.012, 2011.

792    Ghahremaninezhad, R., Norman, A.-L., Croft, B., Martin, R., Leaitch, W. R., Burkart, J., Thomas,
793    J. L., Aliabadi, A. A., Bozem, H., Wentworth, G. R., Murphy, J. G., Levasseur, M., Sharma, S.
794    and Abbatt, J. P. D.: Vertical profile of atmospheric DMS in the Arctic Summer and Spring, ACP
795    prep, 2016.

796    Gibb, S. W., Mantoura, R. F. C. and Liss, P. S.: Ocean-atmosphere exchange and atmospheric
797    speciation of ammonia and methylamines in the region of the NW Arabian Sea, Global
798    Biogeochem. Cycles, 13(1), 161–178, doi:10.1029/98GB00743, 1999.

799    Hegg, D. A., Radke, L. F. and Hobbs, P. V: Particle production associated with marine clouds, J.
800    Geophys. Res. Atmos., 95(D9), 13917–13926, 1990.

801    Heintzenberg, J. and Leck, C.: The summer aerosol in the central Arctic 1991–2008: did it change
802    or not?, Atmos. Chem. Phys., 12(9), 3969–3983, doi:10.5194/acp-12-3969-2012, 2012.

803    Heintzenberg, J., Leck, C., Birmili, W., Wehner, B., Tjernström, M., Wiedensohler, A.,
804    Tjernstrom, M. and Wiedensohler, A.: Aerosol number-size distributions during clear and fog
805    periods in the summer high Arctic: 1991, 1996 and 2001, Tellus B, 58(1), 41–50,
806    doi:10.1111/j.1600-0889.2005.00171.x, 2006.

807    Heintzenberg, J., Leck, C. and Tunved, P.: Potential source regions and processes of aerosol in the
808    summer Arctic, Atmos. Chem. Phys., 15(11), 6487–6502, doi:10.5194/acp-15-6487-2015, 2015.

809    Hoppel, W. a., Frick, G. M., Fitzgerald, J. W. and Larson, R. E.: Marine boundary layer
810    measurements of new particle formation and the effects nonprecipitating clouds have on aerosol
811    size distribution, J. Geophys. Res., 99(D7), 14443, doi:10.1029/94JD00797, 1994.

812    Karl, M., Leck, C., Gross, A. and Pirjola, L.: A study of new particle formation in the marine
813    boundary layer over the central Arctic Ocean using a flexible multicomponent aerosol dynamic
814    model, Tellus B, 64(0), 1–24, doi:10.3402/tellusb.v64i0.17158, 2012.

815    Karl, M., Leck, C., Coz, E. and Heintzenberg, J.: Marine nanogels as a source of atmospheric
816    nanoparticles in the high Arctic, Geophys. Res. Lett., 40(14), 3738–3743, doi:10.1002/grl.50661,
817    2013.

818    Köllner, F., Schneider, J., Bozem, H., Hoor, P., Willis, M. D., Burkart, J., Leaitch, W. R., Abbatt,
819    J. P. D., Herber, A. B. and Borrmann, S.: Particulate Trimethylamine in the summertime Canadian
820    high Arctic, 2016.

821    Kulmala, M., Dal Maso, M., Mäkelä, J. M., Pirjola, L., Väkevä, M., Aalto, P., Miikkulainen, P.,
822    Hämeri, K. and O'Dowd, C. D.: On the formation, growth and composition of nucleation mode
823    particles, Tellus, Ser. B Chem. Phys. Meteorol., 53, 479–490, doi:10.1034/j.1600-0889.2001.d01-
824    33.x, 2001.

825    Kupiszewski, P., Leck, C., Tjernström, M., Sjogren, S., Sedlar, J., Graus, M., M??ller, M., Brooks,
826    B., Swietlicki, E., Norris, S. and Hansel, A.: Vertical profiling of aerosol particles and trace gases
827    over the central Arctic Ocean during summer, Atmos. Chem. Phys., 13(24), 12405–12431,
828    doi:10.5194/acp-13-12405-2013, 2013.

829    Law, K. S. and Stohl, A.: Arctic Air Pollution: Origins and Impacts, Science (80-. )., 315(5818),

Atmospheric
Chemistry
and Physics
Discussions

Open Access

EGU

830    1537–1540, doi:10.1126/science.1137695, 2007.

831    Law, K. S., Stohl, A., Quinn, P. K., Brock, C. A., Burkhart, J. F., Paris, J. D., Ancellet, G., Singh,
832    H. B., Roiger, A., Schlager, H., Dibb, J., Jacob, D. J., Arnold, S. R., Pelon, J. and Thomas, J. L.:
833    Arctic air pollution: New insights from POLARCAT-IPY, Bull. Am. Meteorol. Soc., 95(12),
834    1873–1895, doi:10.1175/BAMS-D-13-00017.1, 2014.

835    Leaitch, W. R., Sharma, S., Huang, L., Toom-Sauntry, D., Chivulescu, A., Macdonald, A. M., von
836    Salzen, K., Pierce, J. R., Bertram, A. K., Schroder, J. C., Shantz, N. C., Chang, R. Y. W. and
837    Norman, A.-L.: Dimethyl sulfide control of the clean summertime Arctic aerosol and cloud, Elem.
838    Sci. Anth., 1(1), 17, doi:10.12952/journal.elementa.000017, 2013.

839    Leaitch, W. R., Korolev, A., Aliabadi, A. A., Burkart, J., Willis, M., Abbatt, J. P. D., Bozem, H.,
840    Hoor, P., Köllner, F., Schneider, J., Herber, A., Konrad, C. and Brauner, R.: Effects of 20-100
841    nanometre particles on liquid clouds in the clean summertime Arctic, Atmos. Chem. Phys.
842    Discuss., 2016(January), 1–50, doi:10.5194/acp-2015-999, 2016.

843    Leck, C. and Bigg, E. K.: Aerosol production over remote marine areas- A new route, Geophys.
844    Res. Lett., 26(23), 3577, doi:10.1029/1999GL010807, 1999.

845    Leck, C. and Bigg, E. K.: Source and evolution of the marine aerosol - A new perspective,
846    Geophys. Res. Lett., 32(19), 1–4, doi:10.1029/2005GL023651, 2005.

847    Leck, C. and Bigg, E. K.: New Particle Formation of Marine Biological Origin, Aerosol Sci.
848    Technol., 44(7), 570–577, doi:10.1080/02786826.2010.481222, 2010.

849    Lohmann, U. and Feichter, J.: Global indirect aerosol effects: a review, Atmos. Chem. Phys., 5,
850    715–735, doi:10.5194/acp-5-715-2005, 2005.

851    Mauritsen, T., Sedlar, J., Tjernström, M., Leck, C., Martin, M., Shupe, M., Sjogren, S., Sierau, B.,
852    Persson, P. O. G., Brooks, I. M. and Swietlicki, E.: An Arctic CCN-limited cloud-aerosol regime,
853    Atmos. Chem. Phys., 11(1), 165–173, doi:10.5194/acp-11-165-2011, 2011.

854    Mungall, E. L., Croft, B., Lizotte, M., Thomas, J. L., Murphy, J. G., Levasseur, M., Martin, R. V.,
855    Wentzell, J. J. B., Liggio, J. and Abbatt, J. P. D.: Dimethyl sulfide in the summertime Arctic
856    atmosphere: measurements and source sensitivity simulations, Atmos. Chem. Phys., 16(11), 6665–
857    6680, doi:10.5194/acp-16-6665-2016, 2016.

858    Nguyen, Q. T., Glasius, M., Sørensen, L. L., Jensen, B., Skov, H., Birmili, W., Wiedensohler, A.,
859    Kristensson, A., Nøjgaard, J. K. and Massling, A.: Seasonal variation of atmospheric particle
860    number concentrations, new particle formation and atmospheric oxidation capacity at the high
861    Arctic site Villum Research Station, Station Nord, Atmos. Chem. Phys. Discuss., 1–41,
862    doi:10.5194/acp-2016-205, 2016.

863    Petters, M. D. and Kreidenweis, S. M.: A single parameter representation of hygroscopic growth
864    and cloud condensation nucleus activity, Atmos. Chem. Phys., 7, 1961–1971, 2007.

865    Pirjola, L., O'Dowd, C. D., Brooks, I. M. and Kulmala, M.: Can new particle formation occur in
866    the clean marine boundary layer?, J. Geophys. Res. Atmos., 105(D21), 26531–26546,
867    doi:10.1029/2000JD900310, 2000.

868    Quinn, P. K. and Bates, T. S.: The case against climate regulation via oceanic phytoplankton

Atmospheric
Chemistry
and Physics
Discussions

869     sulphur emissions, Nature, 480(7375), 51–56, doi:10.1038/nature10580, 2011.

870     Quinn, P. K., Shaw, G., Andrews, E., Dutton, E. G., Ruoho-Airola, T. and Gong, S. L.: Arctic
871     haze: Current trends and knowledge gaps, Tellus, Ser. B Chem. Phys. Meteorol., 59(1), 99–114,
872     doi:10.1111/j.1600-0889.2006.00238.x, 2007.

873     Rehbein, P. J. G., Jeong, C. H., McGuire, M. L., Yao, X., Corbin, J. C. and Evans, G. J.: Cloud
874     and fog processing enhanced gas-to-particle partitioning of trimethylamine, Environ. Sci.
875     Technol., 45(10), 4346–4352, doi:10.1021/es1042113, 2011.

876     Shaw, G. E.: The Arctic Haze Phenomenon, Bull. Am. Meteorol. Soc., 76, 2403–2413,
877     doi:10.1175/1520-0477(1995)076<2403:TAHP>2.0.CO;2, 1995.

878     Skamarock, W. C., Klemp, J. B., Dudhia, J., Gill, D. O., Barker, D. M., Wang, W. and Powers, J.
879     G.: A Description of the Advanced Research WRF Version 2, [online] Available from:
880     http://oai.dtic.mil/oai/oai?verb=getRecord&metadataPrefix=html&identifier=ADA487419
881     (Accessed 22 March 2016), 2005.

882     Stohl, a., Forster, C., Frank, A., Seibert, P. and Wotawa, G.: Technical note: The Lagrangian
883     particle dispersion model FLEXPART version 6.2, Atmos. Chem. Phys. Discuss., 5(4), 4739–
884     4799, doi:10.5194/acpd-5-4739-2005, 2005.

885     Ström, J., Umegård, J., Tørseth, K., Tunved, P., Hansson, H. C., Holmén, K., Wismann, V.,
886     Herber, A. and König-Langlo, G.: One year of particle size distribution and aerosol chemical
887     composition measurements at the Zeppelin Station, Svalbard, March 2000-March 2001, Phys.
888     Chem. Earth, 28(March 2000), 1181–1190, doi:10.1016/j.pce.2003.08.058, 2003.

889     Ström, J., Engvall, A. C., Delbart, F., Krejci, R. and Treffeisen, R.: On small particles in the Arctic
890     summer boundary layer: Observations at two different heights near Ny-Ålesund, Svalbard, Tellus,
891     Ser. B Chem. Phys. Meteorol., 61 B(2), 473–482, doi:10.1111/j.1600-0889.2008.00412.x, 2009.

892     Tjernström, M., Birch, C. E., Brooks, I. M., Shupe, M. D., Persson, P. O. G., Sedlar, J., Mauritsen,
893     T., Leck, C., Paatero, J., Szczodrak, M. and Wheeler, C. R.: Meteorological conditions in the
894     central Arctic summer during the Arctic Summer Cloud Ocean Study (ASCOS), Atmos. Chem.
895     Phys., 12(15), 6863–6889, doi:10.5194/acp-12-6863-2012, 2012.

896     Tjernström, M., Leck, C., Birch, C. E., Bottenheim, J. W., Brooks, B. J., Brooks, I. M., Bäcklin,
897     L., Chang, R. Y. W., De Leeuw, G., Di Liberto, L., De La Rosa, S., Granath, E., Graus, M., Hansel,
898     a., Heintzenberg, J., Held, a., Hind, a., Johnston, P., Knulst, J., Martin, M., Matrai, P. a.,
899     Mauritsen, T., Müller, M., Norris, S. J., Orellana, M. V., Orsini, D. a., Paatero, J., Persson, P. O.
900     G., Gao, Q., Rauschenberg, C., Ristovski, Z., Sedlar, J., Shupe, M. D., Sierau, B., Sirevaag, a.,
901     Sjogren, S., Stetzer, O., Swietlicki, E., Szczodrak, M., Vaattovaara, P., Wahlberg, N., Westberg,
902     M. and Wheeler, C. R.: The Arctic Summer Cloud Ocean Study (ASCOS): Overview and
903     experimental design, Atmos. Chem. Phys., 14(6), 2823–2869, doi:10.5194/acp-14-2823-2014,
904     2014.

905     Tunved, P., Ström, J. and Krejci, R.: Arctic aerosol life cycle: linking aerosol size distributions
906     observed between 2000 and 2010 with air mass transport and precipitation at Zeppelin station, Ny-
907     Ålesund, Svalbard, Atmos. Chem. Phys., 13(7), 3643–3660, doi:10.5194/acp-13-3643-2013,
908     2013.

Atmospheric
Chemistry
and Physics
Discussions

Open Access

EGU

909    Twomey, S.: Pollution and the Planetary Albedo, Atmos. Environ., 41(Vol. 8), 1251–1256,
910    doi:10.1016/j.atmosenv.2007.10.062, 1974.

911    Wang, M. and Overland, J. E.: A sea ice free summer Arctic within 30 years: An update from
912    CMIP5 models, Geophys. Res. Lett., 39(17), 2–6, doi:10.1029/2012GL052868, 2012.

913    Weber, R. J., McMurry, P. H., Mauldin, L., Tanner, D. J., Eisele, F. L., Brechtel, F. J.,
914    Kreidenweis, S. M., Kok, G. L., Schillawski, R. D. and Baumgardner, D.: A study of new particle
915    formation and growth involving biogenic and trace gas species measured during ACE 1, J.
916    Geophys. Res., 103(D13), 16385–16396, doi:10.1029/97JD02465, 1998.

917    Wentworth, G. R., Murphy, J. G., Croft, B., Martin, R. V., Pierce, J. R., Côté, J.-S., Courchesne,
918    I., Tremblay, J.-É., Gagnon, J., Thomas, J. L., Sharma, S., Toom-Sauntry, D., Chivulescu, a.,
919    Levasseur, M. and Abbatt, J. P. D.: Ammonia in the summertime Arctic marine boundary layer:
920    sources, sinks and implications, Atmos. Chem. Phys. Discuss., 15(21), 29973–30016,
921    doi:10.5194/acpd-15-29973-2015, 2015.

922    Wiedensohler, A., Covert, D. S., Swietlicki, E., Aalto, P., Heintzenberg, J. and Leck, C.:
923    Occurrence of an ultrafine particle mode less than 20 nm in diameter in the marine boundary layer
924    during Arctic summer and autumn, Tellus, Ser. B Chem. Phys. Meteorol., 48(2), 213–222,
925    doi:10.1034/j.1600-0889.1996.t01-1-00006.x, 1996.

926    Willis, M. D., Burkart, J., Thomas, J. L., Köllner, F., Schneider, J., Bozem, H., Hoor, P. M.,
927    Aliabadi, A. A., Schulz, H., Herber, A. B., Leaitch, W. R. and Abbatt, J. P. D.: Growth of
928    nucleation mode particles in the summertime Arctic: a case study, Atmos. Chem. Phys., 7663–
929    7679, doi:10.5194/acp-16-7663-2016, 2016.

930    Zhang, J., Spitz, Y. H., Steele, M., Ashjian, C., Campbell, R., Berline, L. and Matrai, P.: Modeling
931    the impact of declining sea ice on the Arctic marine planktonic ecosystem, J. Geophys. Res.
932    Ocean., 115(10), 1–24, doi:10.1029/2009JC005387, 2010.

933

934

Atmospheric
Chemistry
and Physics
Discussions

935



936
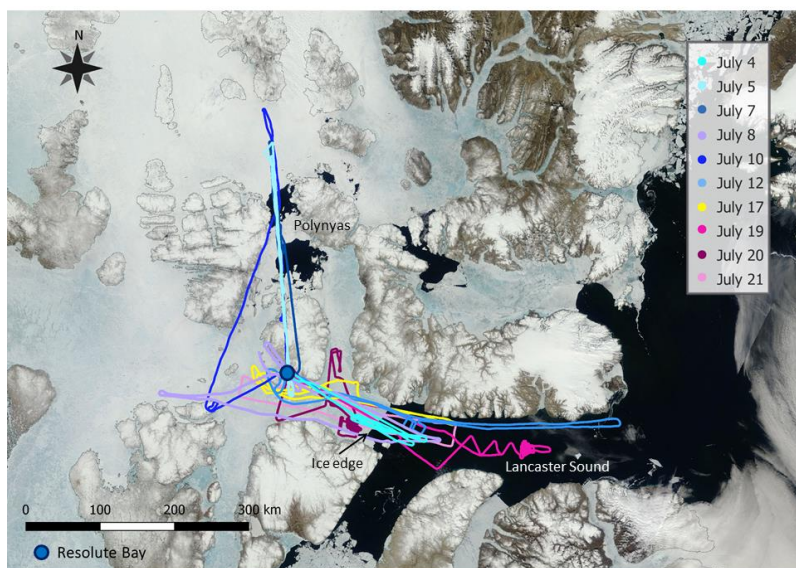
Figure 1. Compilation of all flight tracks plotted on a satellite image from July 4, 2014. The image
is taken from: https://earthdata.nasa.gov/labs/worldview.

939

940
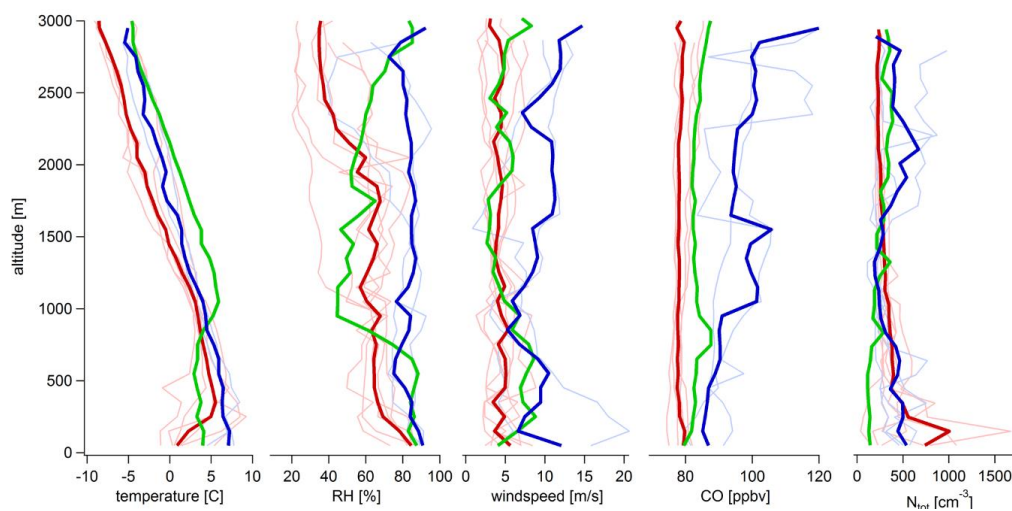
Figure 2. Median temperature, relative humidity (RH), wind speed, CO mixing ratio and $N_{tot}$
profiles for the Arctic air mass period (dark red), the transition day (dark green), and the southern
air mass period (dark blue). Median profiles for each flight are plotted in the background in the
corresponding light colours.
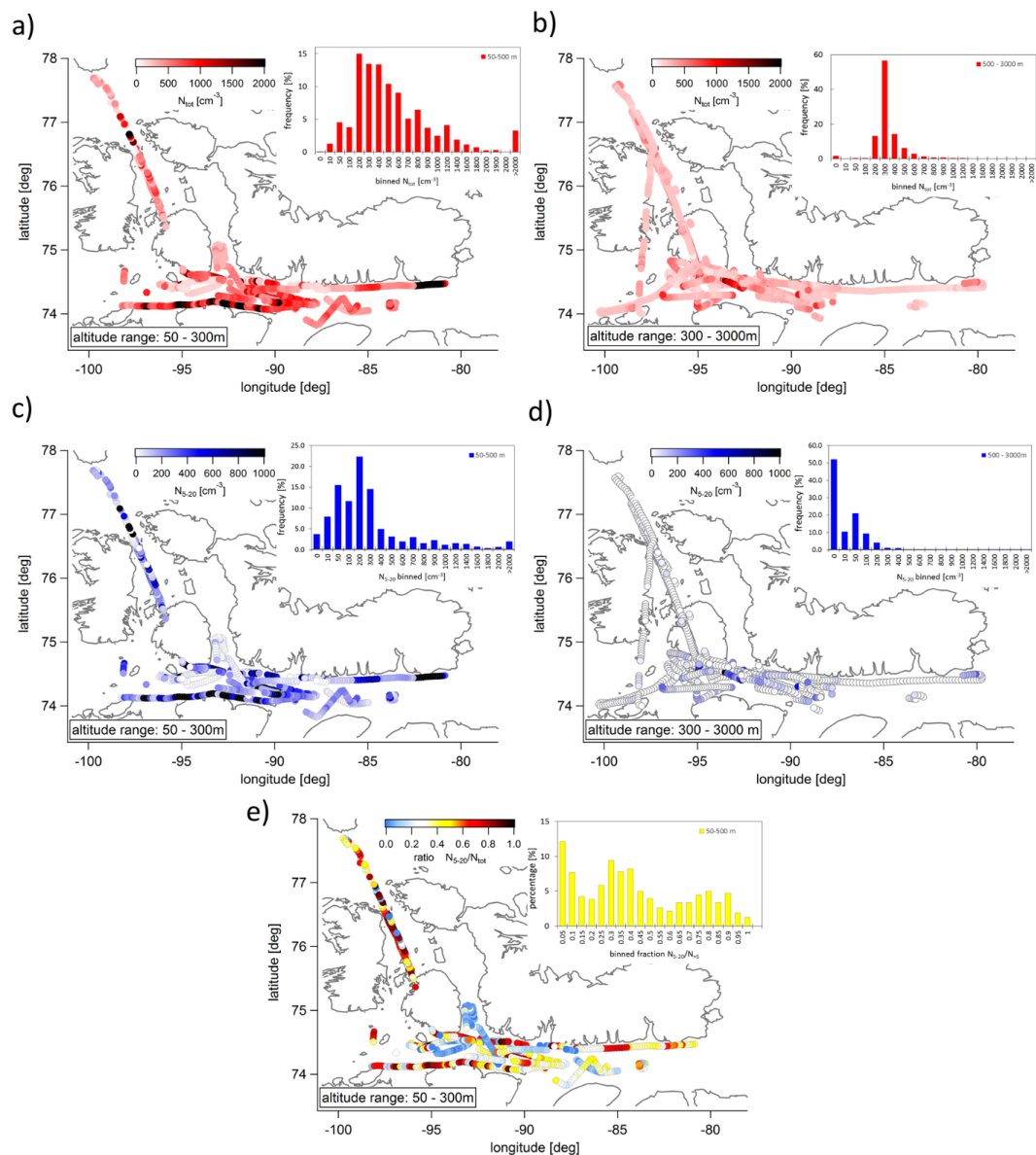
949
Figure 3. Flight tracks colour coded by particle concentrations. a.) Flight tracks within the boundary layer (50-300 m) colour coded by $N_{tot}$. b) Flight tracks within the free troposphere (300-3000 m) colour coded by $N_{tot}$. c) Flight tracks within the boundary layer (50-300m) colour coded by UFP. d) Flight tracks within the free troposphere (300-3000 m) colour coded by $N_{5-20}$. e) Flight tracks within the boundary layer (50-300 m) colour coded by the ratio of $N_{5-20}/N_{tot}$

950
951
952
953
954
955
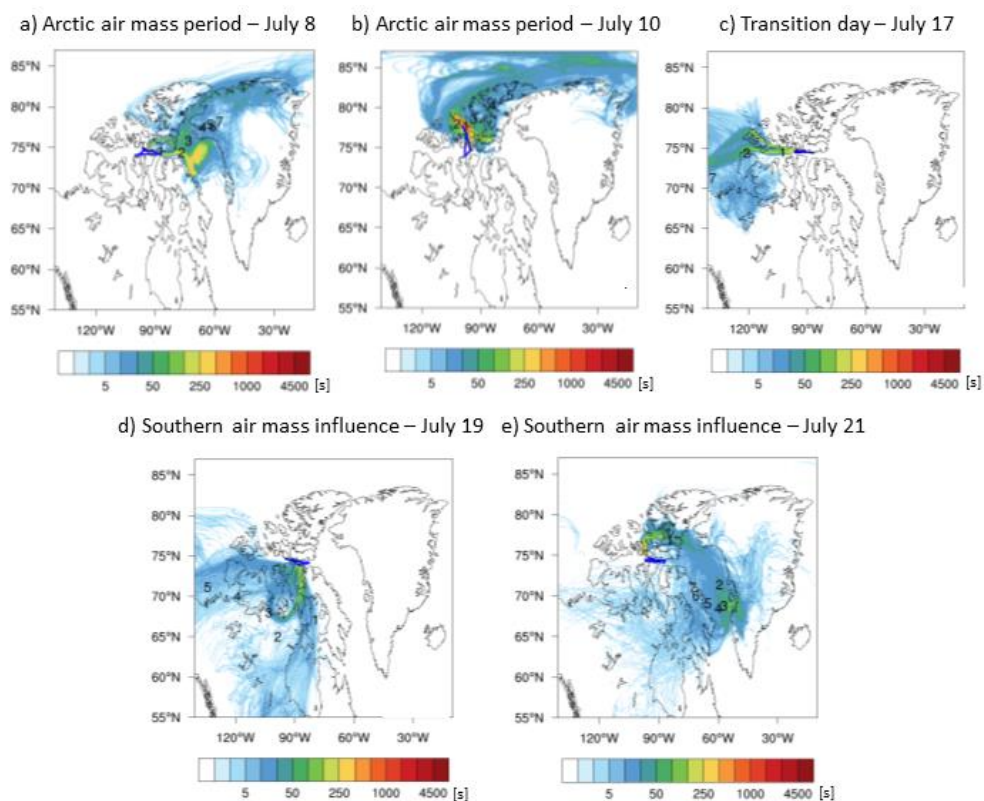
Figure 4. FLEXPART-WRF potential emissions sensitivities for each flight (using particle releases every 2 minutes along the flight track) that illustrate transport regimes during different periods of the campaign. The colour code indicates the residence time of air in seconds and the numbers represent the position of the plume centroid location in days prior to release (days 1-7).

Atmospheric
Chemistry
and Physics
Discussions



962
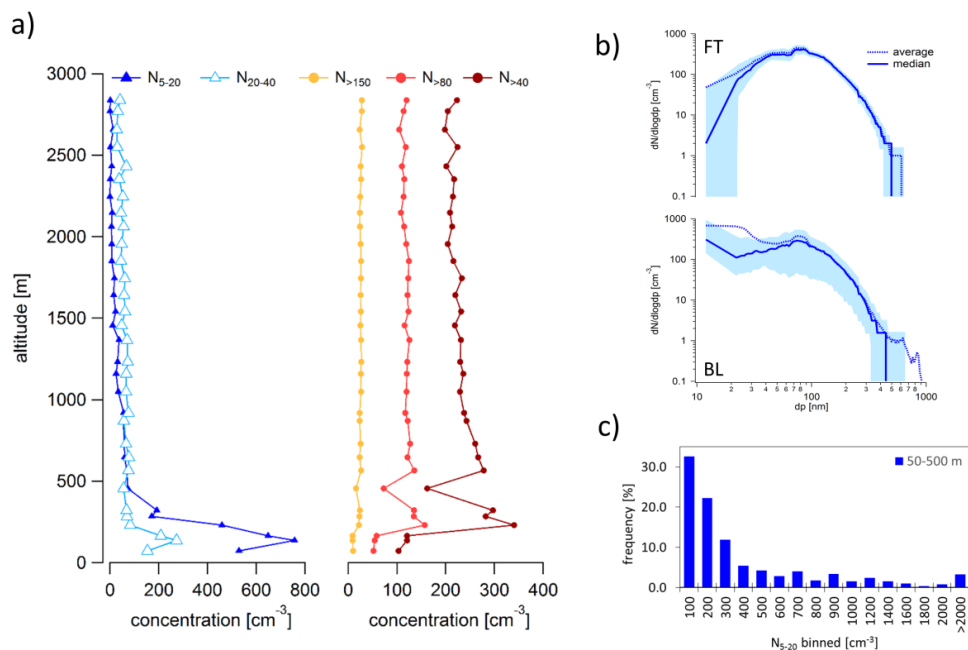
Figure 5. Average particle concentration data during the Arctic air mass period. a) Average vertical profiles of $N_{5-20}$, $N_{20-40}$, $N_{>40}$, $N_{>80}$, and $N_{>150}$. b) Average (solid line) and median (dashed line) size distribution within the BL and the FT. The light blue area represents the 25-75th % percentile range. c) Frequency distribution of the occurrence of UFP illustrates the large variability of the UFP concentrations within the BL.

968

969
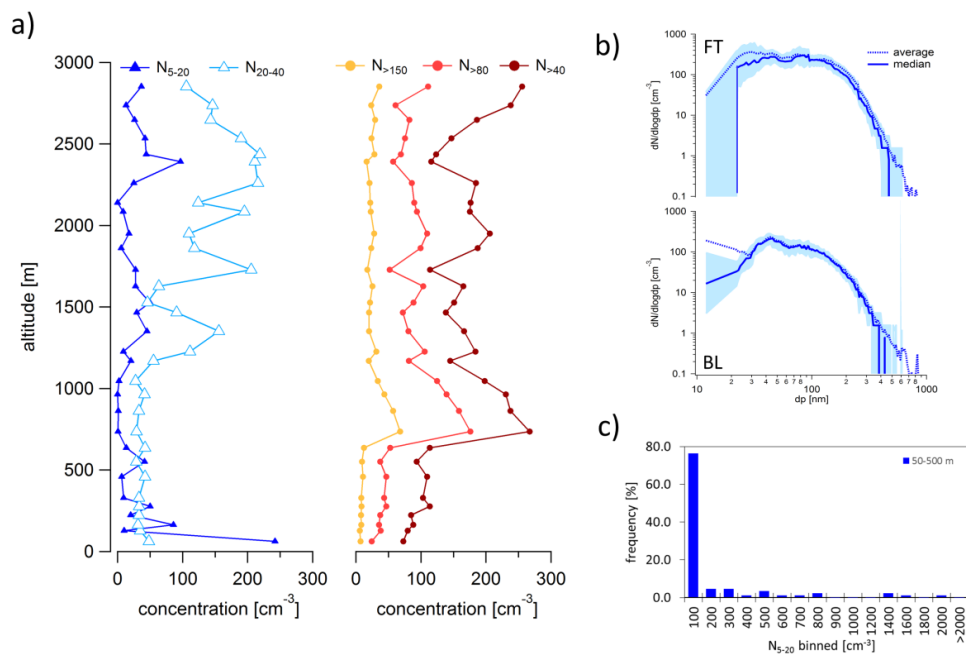
Figure 6. Average particle concentration data on the transition day. a) Average vertical profiles of $N_{5-20}$, $N_{20-40}$, $N_{>40}$, $N_{>80}$, and $N_{>150}$. b) Average (solid line) and median (dashed line) size distribution within the BL and the FT. The light blue area represents the 25-75$^{th}$ % percentile range. c) Frequency distribution of the occurrence of UFP illustrates the large variability of the UFP concentrations within the BL.

975

976
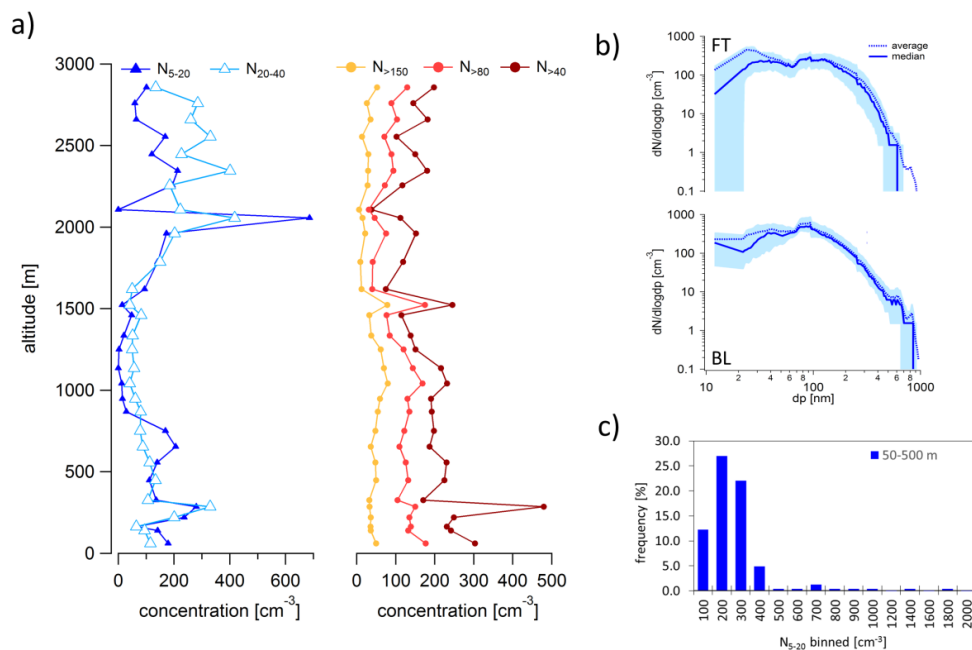
Figure 7. Average particle concentration data during the southern air mass period. a) Average vertical profiles of $N_{5-20}$, $N_{20-40}$, $N_{>40}$, $N_{>80}$, and $N_{>150}$. b) Average (solid line) and median (dashed line) size distribution within the BL and the FT. The light blue area represents the 25-75th % percentile range. c) Frequency distribution of the occurrence of UFP illustrates the large variability of the UFP concentrations within the BL.

982

983

984

985
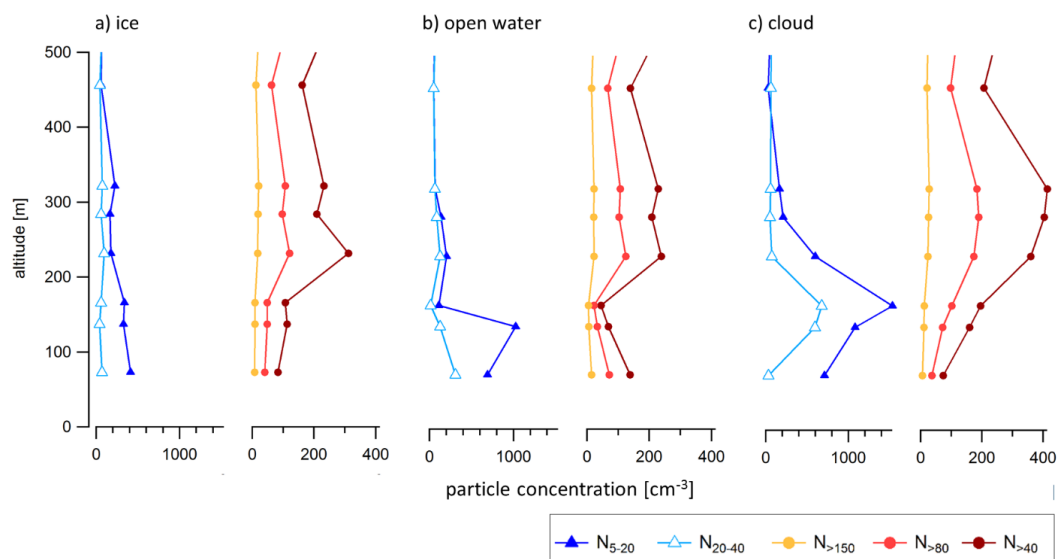
Figure 8. Average profiles of particle concentrations above ice, open water and cloud. The number
of data points for each specific profile is: 130 above water, 216 above cloud, and 123 above water.

988
989

Atmospheric
Chemistry
and Physics
Discussions
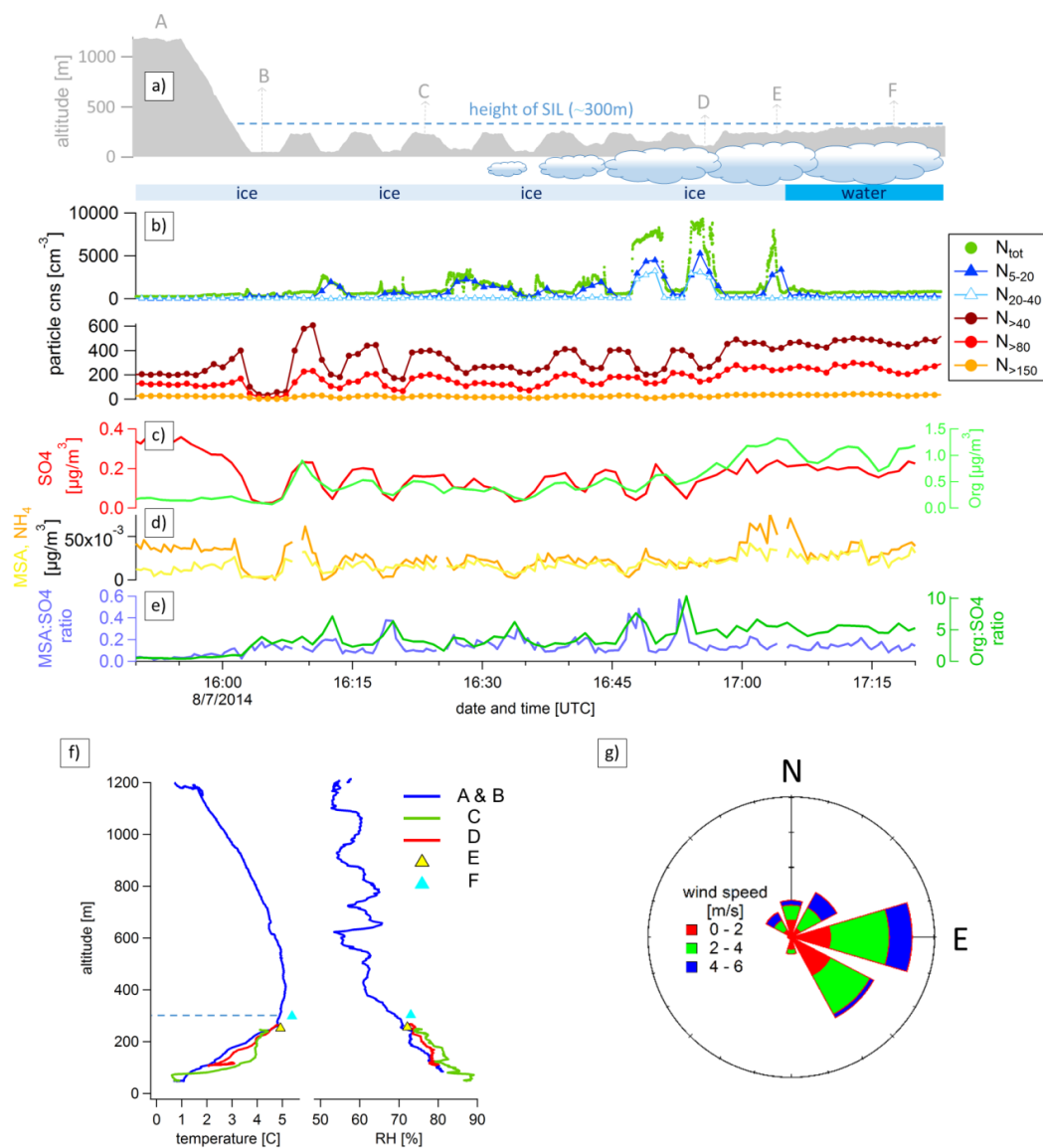


990
991
992 Figure 9. Case study from July 8 flight. Time series of flight altitude and illustration of the surface
993 including cloud coverage (a), aerosol size (b) and chemical composition (c-e). (f) Temperature and
994 relative humidity profile near the locations i-vi (shown in a). (g) Wind direction and wind speed
995 for the entire period
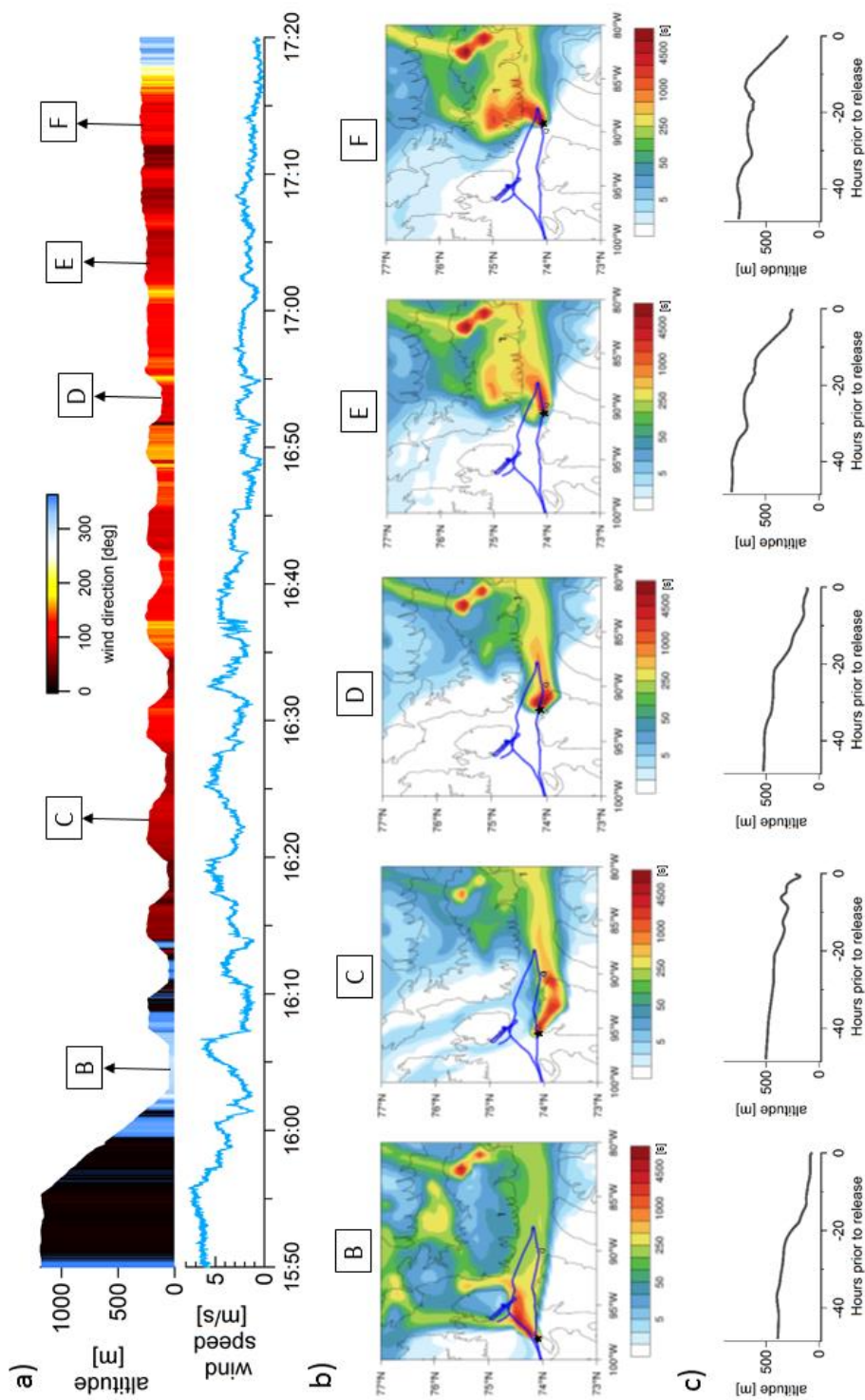
Figure 10. (a) Time series of aircraft altitude color coded with the wind direction and time series of wind speed (b) FLEXPART-WRF seven day backwards potential emissions sensitivities for points along the flight track (60 second release at time at indicated time and location) showing the air mass history at 5 representative locations within the SIL. The plume centroid location for particles with age of one day is indicated. (c) The bottom plots show the altitude of plume centroid 48 hours back in time.

998
999
1000
1001
1002
1003

Atmospheric
Chemistry
and Physics
Discussions

1004
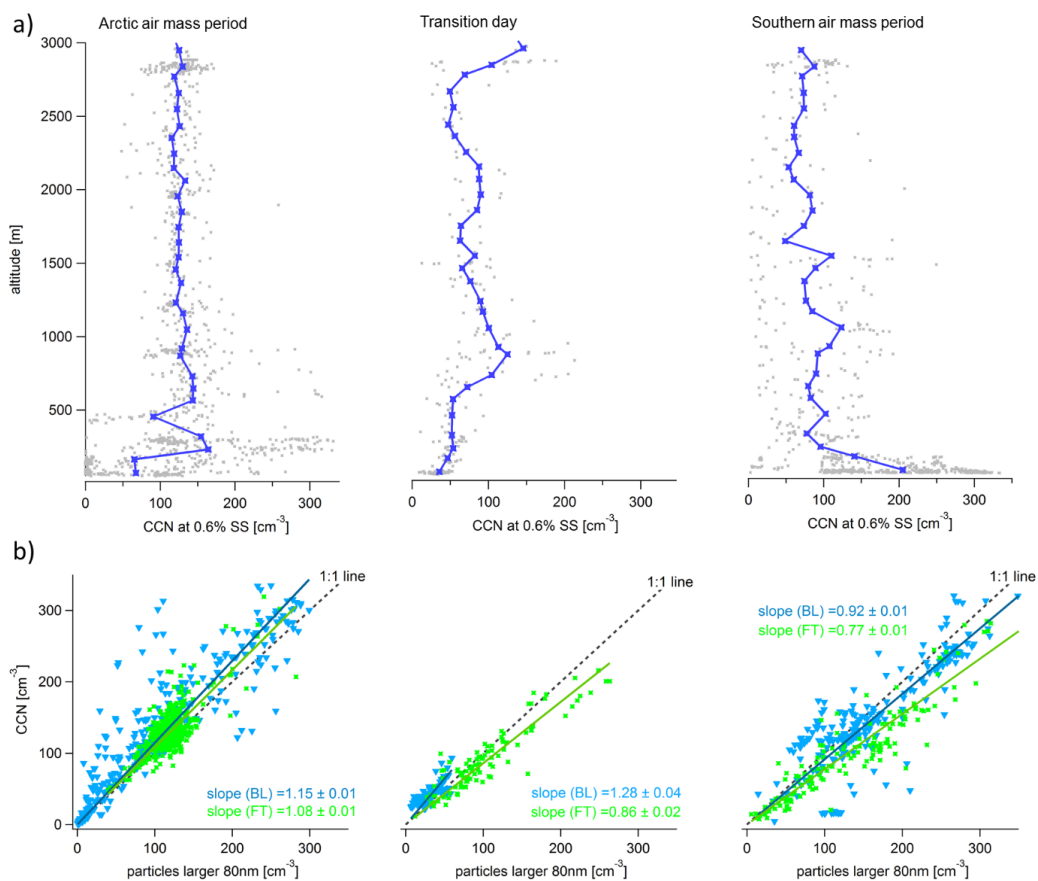


1005

1006   Figure 11. (a) Vertical profiles of average CCN concentrations (dark blue). All data points are
1007   plotted in light grey. (b) Correlation plots between CCN concentrations and particles larger than
1008   80nm.